2006

# Simulation of Steering Systems for Robotic Vehicles

Saurabh Malhotra

THE FLORIDA STATE UNIVERSITY

COLLEGE OF ENGINEERING

# SIMULATION OF STEERING SYSTEMS FOR ROBOTIC VEHICLES

by

SAURABH MALHOTRA

A Thesis submitted to the
Department of Mechanical Engineering
in partial fulfillment of the
requirements for the degree of
Master of Science

Degree Awarded
Spring Semester, 2006

The members of the committee approve the thesis of Saurabh Malhotra defended on 03/20/2006.

_____
Patrick Hollis,
Professor Directing Thesis

_____
Carl Moore
Committee member

_____
Juan Carlos Ordonez
Committee member

**APPROVED:**

_____
Chiang Shih, Chair, Ph.D., Department of Mechanical Engineering

_____
C. J. Chen, Ph.D., Dean, FAMU- FSU College of Engineering

The office of Graduate Studies has verified and approved the above named committee members

# ACKNOWLEDGEMENT

I would like to take this opportunity to thank a few of the many people who have made my graduate studies and this thesis possible. To them and many others I am truly grateful. First of all, I would like to express my deepest gratitude to my advisor, Dr. Patrick Hollis for his technical guidance and financial support throughout my research. I found my research and work place so enjoyable because of his invaluable supervision and constant encouragement.

I would also like to thank Dr. E Collins for serving in my graduate committee and for introducing me to the world of robotics. Special thanks to financial support provided by Robotics research lab at FAMU – FSU College of engineering. This thesis wouldn't be possible without it. I am thankful to Dr. Farrukh Alvi (Graduate Coordinator) for providing me an opportunity to study in Graduate school at Florida State University. I owe special gratitude to Naveen and Anindya for being such nice friends and for helping in my research. They were of immense help and support to me. They made my stay in Tallahassee very pleasant and rich. I feel very privileged to have worked with so many nice people at Florida State University.

I feel most indebted to my Father who taught me the importance of education in life and to my mother who gave me the courage to face and overcome new challenges. It wouldn't have been possible to come to U.S.A for graduate studies without love and support of my brother Prateek and my friend Rohit. Without them none of my dreams would have become reality. This thesis is dedicated to all these most important people in my life.

# TABLE OF CONTENTS

# LIST OF FIGURES

# NOMENCLATURE

| | |
|---|---|
| $Fy_f$ | Lateral force on the front tire |
| $Fy_r$ | Lateral force on the rear tire |
| $Fx_f$ | Longitudinal force on the front tire |
| $Fx_r$ | Longitudinal force on the rear tire |
| $\delta_f$ | Steering angle of the front wheel |
| $\delta r$ | Steering angle of the rear wheel |
| m | Mass of the vehicle |
| r | Yaw rate |
| $v_x$ | Longitudinal velocity |
| $v_y$ | Lateral velocity |
| $Lf$ | Distance of the center of gravity from the front wheel |
| $Lr$ | Distance of the center of gravity from the rear wheel |
| $R_w$ | Wheel radius |
| $I_w$ | Inertia of the wheel about the axle |
| $Ta_f$ | Applied throttling torque for the front wheel |
| $Tb_f$ | Applied braking torque for the front wheel |
| $\frac{dw_f}{dt}$ | Angular velocity of the front wheel |
| $\frac{dw_f}{dt}$ | Angular velocity of the rear wheel |
| $Ta_r$ | Applied throttling torque for rear wheel |
| $Tb_r$ | Applied braking torque for rear wheel |
| $v_X$ | Longitudinal velocity component with respect to fixed inertial coordinates |
| $v_y$ | Lateral velocity component with respect to fixed inertial coordinates |

| | |
|---|---|
| $v_x$ | Longitudinal velocity component with respect to the moving coordinates |
| $v_y$ | Lateral velocity component with respect to the moving coordinates |
| $Fz_f$ | Front normal loads |
| $Fz_r$ | Rear normal load |
| $a_x$ | Instantaneous Longitudinal acceleration |
| h | Height of the car CG from the ground |
| $\alpha_f$ | Slip angle of the front wheel |
| $\alpha_r$ | Slip angle of the rear wheel |
| $Vtf$ | Front axle velocity |
| $Vtr$ | Rear axle velocity |
| $v_{wxf}$ | Longitudinal component of the front tire velocity |
| $v_{wxr}$ | Longitudinal component of the rear tire velocity |
| $S_{af}$ | Longitudinal Slip of the front tire |
| $S_{ar}$ | Longitudinal Slip of the rear tire |

# ABSTRACT

Robotic tasks involves a range of steering activity: one application is highway driving with very little turning for hundreds of kilometers; another is steering for military robots which requires more flexible turning and maneuvering. Modeling and simulation are more widely used in robotic vehicle engineering to reduce development time, improve the design and to reduce the complexity of the robotic vehicle. This thesis mainly focuses on steering system modeling and simulation. It also reviews different types of steering systems that are used for robotic vehicles and military robotic vehicles such as the XUV. Steering systems that are modeled and simulated are skid steering and four wheel steering. A mathematical model of XUV steering system is developed in Matlab and various simulations are performed using the mathematical model. It is followed by a Matlab simulation of the using a state space representation. Results of the Matlab simulation are compared to the results obtained from an ADAMS simulation of the solid model of the XUV. Then the concept of four wheel steering is introduced for the XUV. A Matlab simulation of this model is done to check the stability of the system. It is followed by vehicle handling characteristics of the XUV for the four-wheel steering system and its Matlab simulation. The results of dynamic motion analysis are discussed for future research.

# CHAPTER 1

# INTRODUCTION

## 1.1 Mobile robotics research history

Mobile robotics research has played a very important role in the application of robots in this world. At Stanford University, Nils Nilson[1] developed the mobile robot SHAKEY in 1969. This robot possessed a camera, binary tactile sensor and a visual range finder. This was the first mobile robot which used artificial intelligence to control its actions. The main objective of this mobile robot was to maneuver in complicated environments such as office buildings. The JPL lunar rover [2], developed in 1970 at the Jet Propulsion laboratory, was developed for planetary exploration. With the help of a TV camera, laser range finder, and tactile sensors, the robot categorized its environment as traversable, not traversable, and unknown. In the late 1970s Hans Moravec [3] developed CART in the Artificial Intelligence laboratory at Stanford. The robot was capable of following a white line on a road. A television camera which was mounted on a rail on the top of CART took pictures from several different angles and relayed them to a computer, which performed obstacle avoidance by gauging the distance between CART and obstacles in its path. In 1994, the CMU Robotics Institute's Dante II [4], a six-legged walking robot, explored the Mt. Spurr volcano in Alaska to sample volcanic gases. In 1997 NASA's Mars Pathfinder delivered the Sojourner rover [5] to Mars. Sojourner sent back images of its travels on the distant planet. Also in this same year, Honda showcased the P3 [6], an extraordinary prototype in humanoid robotic design. Currently NASA’s rovers SPIRIT and OPPORTUNITY [7] are exploring the Martian soil for signs of water.

## 1.2 Importance of mobile robotics research

Autonomous mobile robotics is a challenging research topic for several reasons. First, to change a mobile robot from a computer on wheels able to sense some physical properties of its environment into an intelligent machine, able to identify features, detect patterns, learn from experience, build maps, and navigate requires the simultaneous application of many research disciplines. Engineering and computer science are core disciplines of mobile robotics. When questions of intelligent behavior arise, cognitive science, psychology and to some extent philosophy also offer hypotheses and answers.

Second, autonomous mobile robots are the closest approximation yet of intelligent agents. For centuries people have been interested in building machines that can think and make decisions based on the environment around them. To satisfy this goal mobile robotics research has increasingly incorporated artificial intelligence enabling the machines to mimic living beings.

Third, there are many applications for mobile robots. Transportation, surveillance, inspection, cleaning and entertainment are just some examples. Mobile robots have been used for outdoor security applications like the PatrolBot [8] by ActiveMedia. There are robotic vacuum cleaners like ROOMBA [9] by iRobot and robotic animals like Sony's Aibo [10]. There are several mobile robotics applications for environments that are inaccessible or hostile to humans. For example mobile robots are used for underwater exploration, bomb disposal, and cleanup of contaminated environments. Finally, there are military applications for mobile robots. Packbot [11] by iRobot, has been used in the 2001 war in Afghanistan. DARPA's Micro Air Vehicles (MAVs) [12] and General Dynamics Sentinel Robots [13] have been made for the US Army for deployment on the battlefield. Before the infantry moves in, these robots can scan the area for information regarding the terrain, enemy camp positions, and weather conditions.

## 1.3 Research Objective

The Experimental Unmanned Vehicle (XUV) [14], shown in Figure 1.1, was developed by General Dynamics Robotic Systems for the US Army. It is a semi-autonomous

unmanned ground vehicle (UGV) that uses high fidelity sensors for reconnaissance, surveillance, and target acquisition. It is an all terrain vehicle with a payload of 2500 lbs, capable of road following at 40 mph and obstacle avoidance. The XUV has a sensor suite comprised of wheel encoders, an inertial reference unit (IRU) for navigation, GPS, a laser range finder, mono and stereo cameras, wireless LAN antenna, and PLGR remote antenna.


Figure 1.1: XUV

The current goal of XUV research is to develop autonomous mobility that enables an UGV to maneuver over rugged terrain as part of a mixed manned and unmanned vehicle group. As part of this goal, the XUV must be able to maneuver at speeds higher than traditional UGVs. For this, the vehicle controller needs to know steering commands to determine how the steering system will behave under different conditions such as changes in the velocity of the vehicle, changes in tire properties, changes in motion, close to tipping etc.

### 1.4 Elements of robotics research

Mobile robotics research can be studied as a combination of following areas

1) Advanced perception

2) Advanced controller architecture
3) Vehicle dynamic modeling, simulation and experimentation

This thesis basically focuses on mathematical modeling, 3d modeling and simulation. ADAMS and Pro/E are used for dynamic modeling; Matlab and Simulink are used for theoretical simulations. The later part of this research is to extend these mathematical models of the XUV type of vehicles which are basically used for the Army applications. This Research focuses on three of these areas:

1) Mathematical modeling and simulation of the steering system used in the XUV
2) Dynamic modeling and simulation of XUV steering using ADAMS
3) Computer simulation of four wheel steering

Steering characteristics and their steering geometry are discussed along with different parameters on which the performance of the steering system depends. Different types of steering mechanisms are compared on the basis of maneuverability, power requirements and control systems involved. Mathematical modeling of the steering system used in XUV type of vehicle is done and simulations are performed using Matlab and Simulink software. Results obtained from these simulations are compared with the results of dynamic simulations performed on the XUV type of vehicle in ADAMS software.

**1.5 Chapter Summaries**

This chapter gives a very brief history and overview of current applications of mobile robotics, describes past research done in this area and summarizes our research objectives. Chapter 2 explains some of the steering concepts used by the ATRV jr robot and the XUV vehicles .Chapter 3 presents the mathematical modeling of the steering system using a bicycle model .Chapter 4 contains the simulation results for the XUV type of vehicle. Chapter 5 contains the Matlab simulation results, the comparison of the various simulation results with, helps to describe the behavior of XUV vehicle in different conditions. It summarizes the contributions of this research and proposes future work.

# CHAPTER 2

# STEEERING SYSTEM USED IN ROBTOIC VEHICLES

## 2.1 Introduction to Steering Concepts

This chapter mainly concentrates on the steering fundamentals and the concept of Instantaneous Center of Rotation (ICR), figure (2.1).

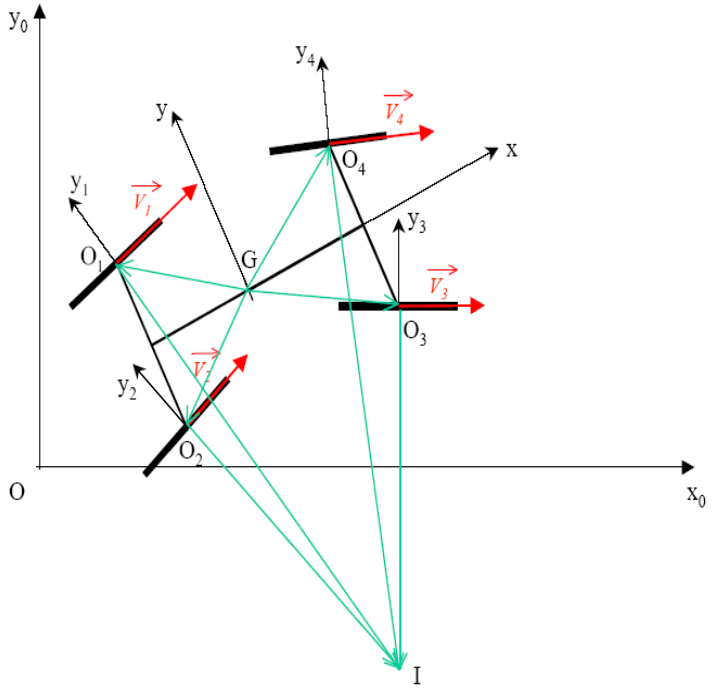


**Figure 2.1: ICR Concept**

The axles of the wheels intersect at a point if there is no slipping. Each wheel rolls without slip about this intersection point. The point I is the Instantaneous Center of Rotation (ICR) for vehicle movement relative to the surface.

## 2.2 Trailer Vehicle Steering Study

In this type of vehicle, figure (2.2), the wheels A-B and C-D have the same rotation axis. The instantaneous rotation center is located at the intersection of (A or B) and (C or D)

wheel axes. All four wheels of this type of vehicle are independent of each other in order to have different rotational velocities. Then $V_A \neq V_B \neq V_C \neq V_D$. This means that if the vehicle is rear wheel drive, a differential is needed between the two rear wheels. If the vehicle is four wheel drive, two more differentials are required.

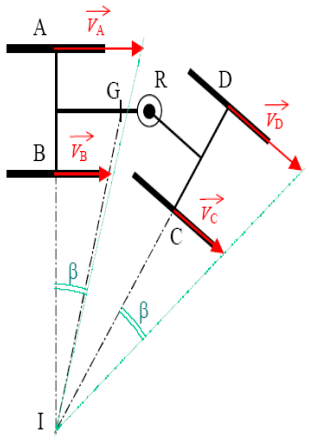


**Figure 2.2: Geometric Analysis**

### 2.3 Four Wheeled, two wheels steering study

If the steering wheels remain parallel during steering as shown in figure (2.3), then there is no single intersection point; this is incompatible with the no slip hypothesis. In this case of steering, at least one velocity vector has to have a different direction .This means that at least one wheel slips to allow the vehicle to move. A solution is to use a different steering angle for each steering wheel. The angle between steering wheels is called Ackerman steering angle.

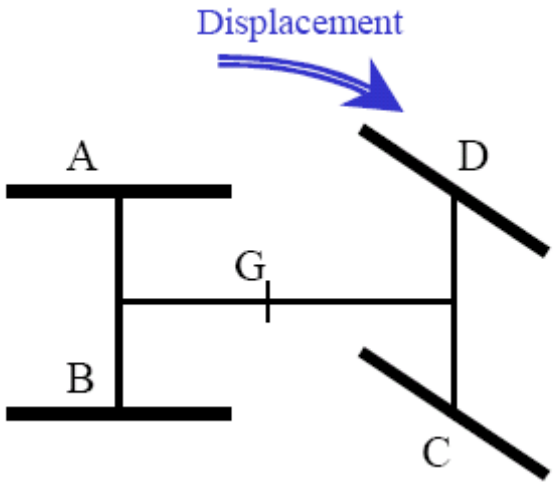


**Fig 2.3: Four Wheeled, two steering wheels**

### 2.4 Non Parallel steering wheels

With the proper steering angles, figure (2.4), the instantaneous rotation center exists and can be found in the same way as previously described. The instantaneous rotation center is situated at the intersection of A (or B) and C (or D) wheel axes. Assuming no slip the differential steering angle must be such that the three wheel axes intersect at the same point (ICR) .Note: the four wheels have to be independent so that each wheel can rotate at different velocities. This means that if the vehicle is rear wheel drive, a differential is needed to between the rear wheels. If it is four wheel drive, two more differentials are needed.

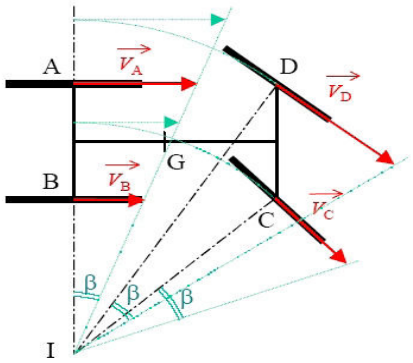


**Figure 2.4: Non parallel Steering**

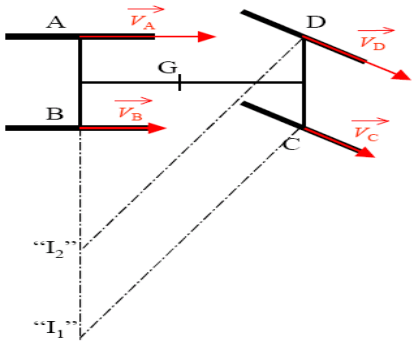


**Figure 2.5: Parallel Steering kinematics study**

### 2.5 Four wheeled vehicle with four steering wheels

As shown in the figure (2.6), in this type of steering system, all the four wheels of the vehicle can be steered at the same time.

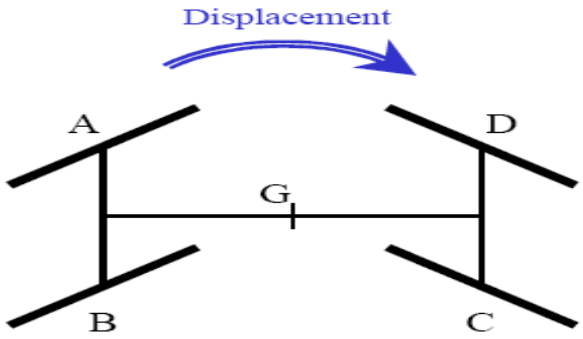


**Figure 2.6: Four Wheeled Vehicle with four Steered wheels**

### 2.6 Parallel steering study

If the steered wheels remain parallel during steering, figure (2.7), there is no single intersection point .This is incompatible with the hypothesis of no slip. In this case, at least two velocity vectors must have different directions. This means at least two wheels slip in order to make the vehicle move.

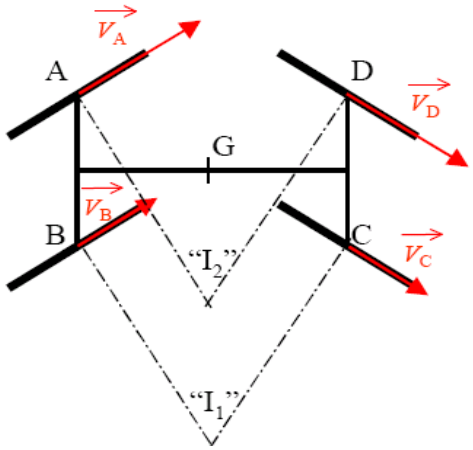


**Figure 2.7: Four wheeled vehicle with parallel steering**

## 2.7 Non-parallel Steering

With the proper steering angles, the instantaneous rotation center exists and can be found, Figure (2.8). This kind of steering system permits the vehicle to have an ICR located anywhere in the plane, Figure (2.9). The differential steering angles must be set correctly to get a single instantaneous rotation center.

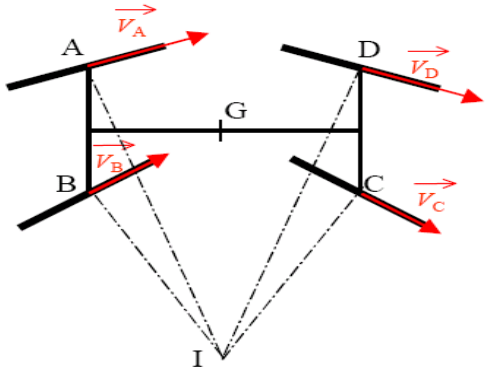


**Figure 2.8: Four wheeled vehicle with nonparallel steering**

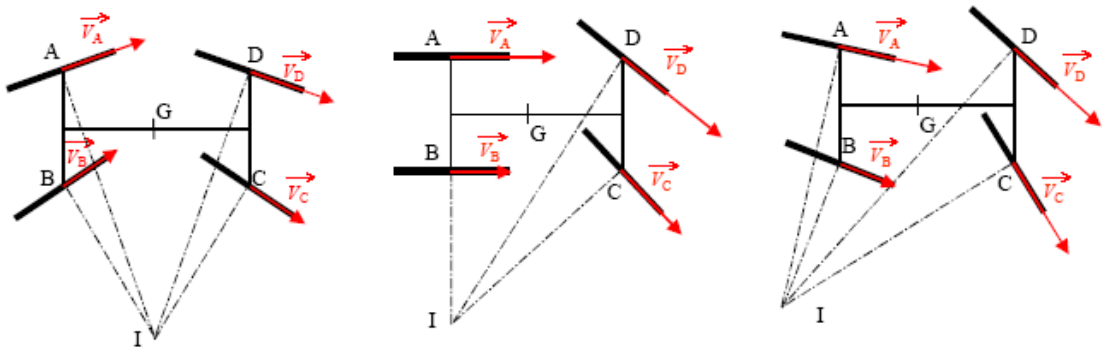


**Figure 2.9: Arbitrary location of IRC for nonparallel steering**

There are some special cases that require separate attention, figure (2.10).

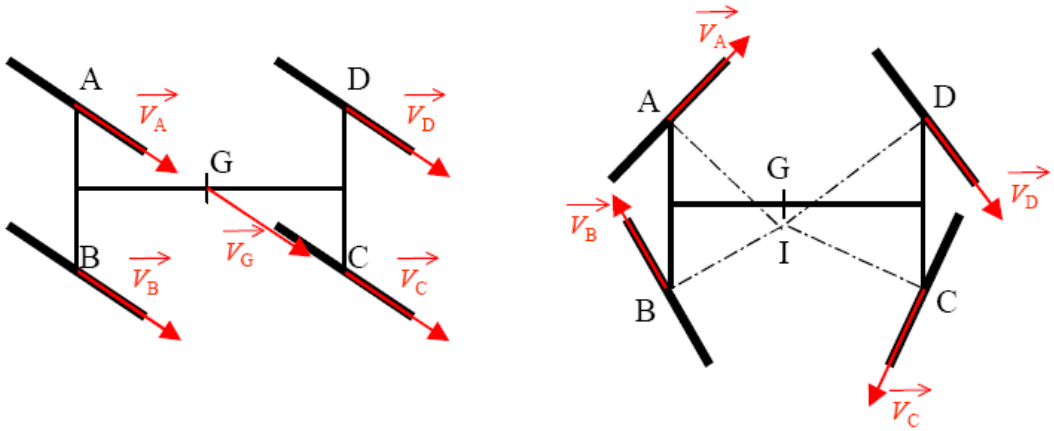


**Figure 2.10: Special cases of nonparallel steering**

### 2.8 Three wheeled robot steering study

Again assume that there is no slip, figure (2.11). Each wheel velocity is perpendicular to its rotation axis. In this case, wheels A and B have the same rotation axis. The instantaneous rotation center is located at the intersection of A (or B) and C wheel axes. In this case $V_A \neq V_B \neq V_C$. The three wheels have to be independent so that they rotate at different rotational speeds. This implies that if the three-wheeler is rear wheel drive, a differential is needed between the rear wheels. If there are three driving wheels, a second differential is required between front and the rear.

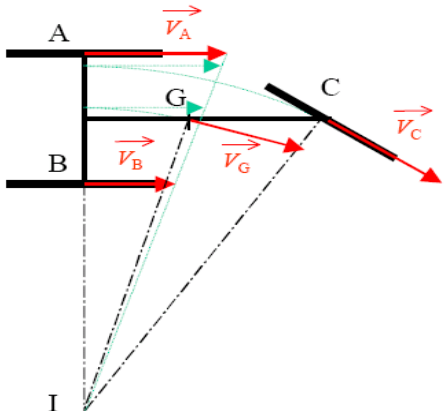


**Figure 2.11: Three wheeled mobile robot steering**

## 2.9 Potential Robotic Vehicle Steering Systems

The XUV vehicle is used for military applications such as combat operations, reconnaissance and maneuvering on uneven terrains (sand, mud, gravel or ice). There are different types of steering systems possible for such robotic vehicles.

1) Skid Steering: skid steering or differential steering, figure (2.12), uses parallel sets of wheels or tracks on either side of the vehicle. In order to generate a turn the wheels on each side of the vehicle are driven with different velocities. The different velocities define the turning radius. Symmetrical design usage and driving the wheels/tracks on either side at equal velocities in opposite directions will cause the robot turning center to coincide with its geometric center.

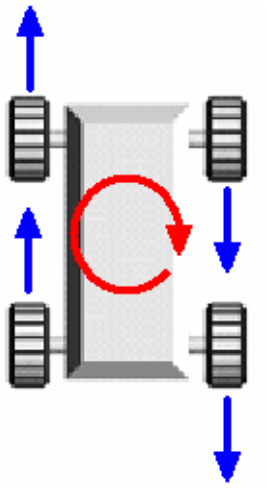

**Figure 2.12: Skid Steering performing point turn**

This provides high maneuverability as the robotic vehicle is capable of turning at the fixed point without many complexities. Skid steering is compact, requires few parts and exhibits agility from point turning to line driving using only the components, motions and swept volume needed for straight line driving. The major disadvantage is the power required to take a turn, especially from a stationary position as the wheels must move in the lateral direction as well as forward. This increases the power consumption and forces the design to withstand wear and tear on the tires/tracks. Skid steering is therefore most suitable for robotic applications involving rough terrain, and/or terrain with loose or soft surfaces. Skid steering is an effective solution to the steering problem in robotic vehicles. A skid steered vehicle which is symmetric about its axis has an advantage of equal maneuverability whether it is in a forward or reverse direction.

2) Articulated steering: In order to turn a four wheeled vehicle with minimum lateral force on the tires, the outside tires must turn with a larger radius compared to the inner tires. This can be accomplished by articulated steering where a piece of the chassis or axle is hinged as shown by figure (2.13). The robotic vehicle steers by folding the joint, providing each wheel with a heading tangent to a circle centered on the turn center.

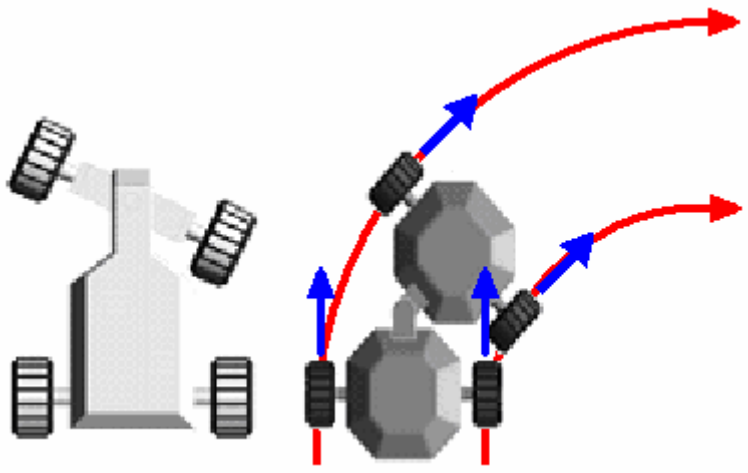

**Figure 2.13: LEFT: Articulated axle; RIGHT: Articulated Frame**

The efficiency of articulated steering is much higher than that of skid steering; however the turning radius is larger, which reduces the maneuverability. The mechanical design is

still very simple. Basically the drive is applied to two wheels from a single motor. This requires a differential to be used in order to allow the inside wheel to travel a shorter distance than the outer wheel.

3) Ackerman Steering: This is another method of steering which overcomes the problem of the inside and outside radii being different; reducing the forces on the tires. This is the most common type of steering mechanism used in automobiles. The tires remain at a fixed pivot position but turn to different angles on each side of the vehicle as given by figure (2.14).

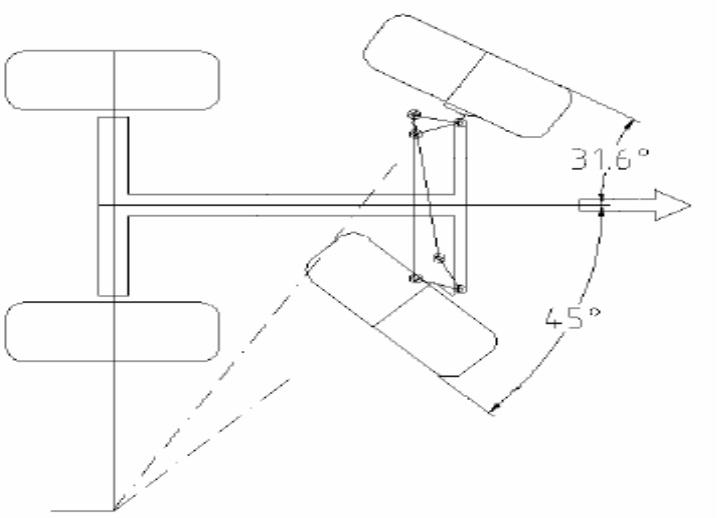


**Figure 2.14: Ackerman Steering**

Since the tire angles required depend on the chassis design, each robotic vehicle must be uniquely designed. Most mechanical designs are not able to match the requirements exactly, but offer a close approximation. As the turning radius is large the maneuverability of this system is low. By turning the front and rear sets of wheels, the turning radius can be reduced .Another alternative is to drive backwards so that rear set of wheels will be responsible for steering.

4) Independent or explicit steering: This involves independently steering each wheel as shown in figure (2.15). It allows maximum flexibility of movement for a wheeled

vehicle. The system can perform both Ackerman and skid steering techniques. Control and accuracy of the steering angles makes the design more complex and expensive; however the maneuverability of the system is extremely high, especially in confined spaces.

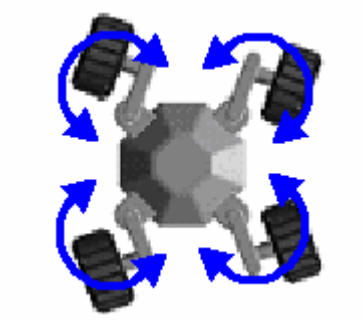

**Figure 2.15: Independent Explicit Steering**

A four-wheeled vehicle has the potential to perform point turns by turning all of the wheels perpendicular to radial lines emanating from its geometric centre. This is very efficient as the wheels experience no lateral forces. A unique advantage of independent steering is the ability to "crab steer". This is achieved by setting all of the wheels to face in the same direction so that the vehicle can drive sideways with respect to the chassis. Usually all the wheels are driven ,so a four wheel vehicle requires four motors for steering and four motors for driving the wheels.

Figure (2.16) summarizes the major steering types available for use in robotic vehicles.

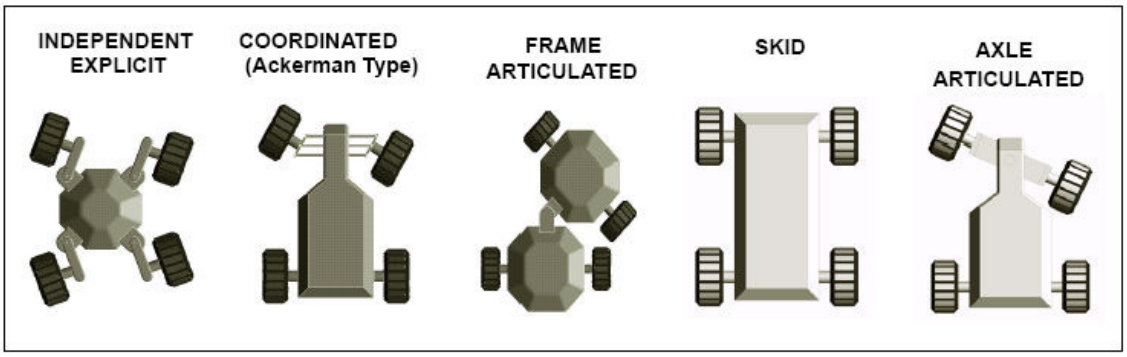


**Figure 2.16: Kinematics of major steering types**

# CHAPTER 3

## MATHEMATICAL MODELLING OF STEERING SYSTEM

Mathematical modeling and Simulations is very useful in robotics engineering, and there are various ways for both building dynamic model and for interfering with these models. Dynamic and Kinematics modeling are used extensively in order to develop and extend the understanding of ground vehicle handling and stability. The dynamic and kinematics models must include the various parameters involved in vehicle steering like the mass, inertia of wheels, steering angle, vehicle slip, and traction effects in land vehicles. Basic vehicle dynamics involve lateral/directional and longitudinal motions. Lateral/directional dynamics basically refers to vehicle responses, which include yaw and rolling motions. Longitudinal dynamics involve speed response and pitching and heave motions due to longitudinal and vertical tire forces as induced by engine power and braking. The formation of Mathematical model helps in understanding the traction effects that exists between vehicle tire and road surface, which forms the basis of theoretical Simulation modeling. The XUV used for modeling and Simulation is a four wheeled, four wheel Ackerman-steered, all-wheel drive autonomous vehicle that is approximately 10 feet long, 5 feet wide, 4 feet high and having a curb weight around 3000 pounds. A dynamic model is described using a basic standard bicycle model, which has five degrees of freedom. Here we are basically concerned with the Simulation of Steering System used in XUV type of vehicle.

**Fig (3.1): An XUV vehicle (Source: www.isd.mel.nist.gov)**

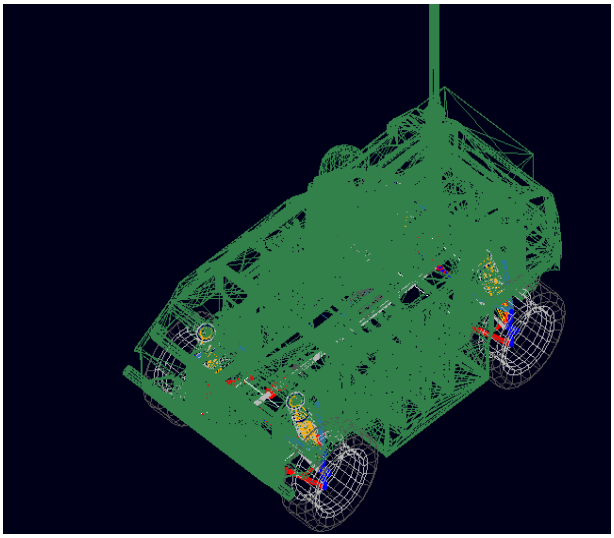

***Fig (3.2): XUV from ADAMS Software***

### 3.1 Mathematical Modeling and Equations of motion

The following assumptions are made:

1) The vehicle is moving on a fixed horizontal frame
2) Vehicle is moving at a very low speed
3) Longitude slippage is neglected
4) Lateral force on the tire is directly proportional to the vehicle load
5) Wheel actuation is equal on each side in order to reduce the longitudinal slip
6) Vehicle is rotating in counterclockwise direction

This chapter covers the dynamic modeling of the vehicle, including the effects of Weight transfer and road bank. Section 3.2 covers the basic mathematical modeling of the vehicle's non-linear lateral and roll dynamics, as well as assumptions made in order to linearlize the model.

### 3.2 Vehicle Modeling

The vehicle schematic shown in Figure 3.3 is a simple diagram of a four wheel Vehicle in the lateral and longitudinal planes. In order to simplify the lateral dynamics, the longitudinal dynamics, including drive force and rolling resistance, were neglected. Additionally, the front and rear track widths ($t$) are assumed to be equal. As seen in Figure 3.3, the sideslip ( $\beta$) of the vehicle is the difference between the velocity heading ( $\nu$) and the true heading of the vehicle ( $\psi$). The yaw rate ($r$) is the angular velocity of the vehicle about the center of gravity. The lateral forces ($F_y$) are shown for both the inner and outer tires as well as the front and rear tires of the vehicle.

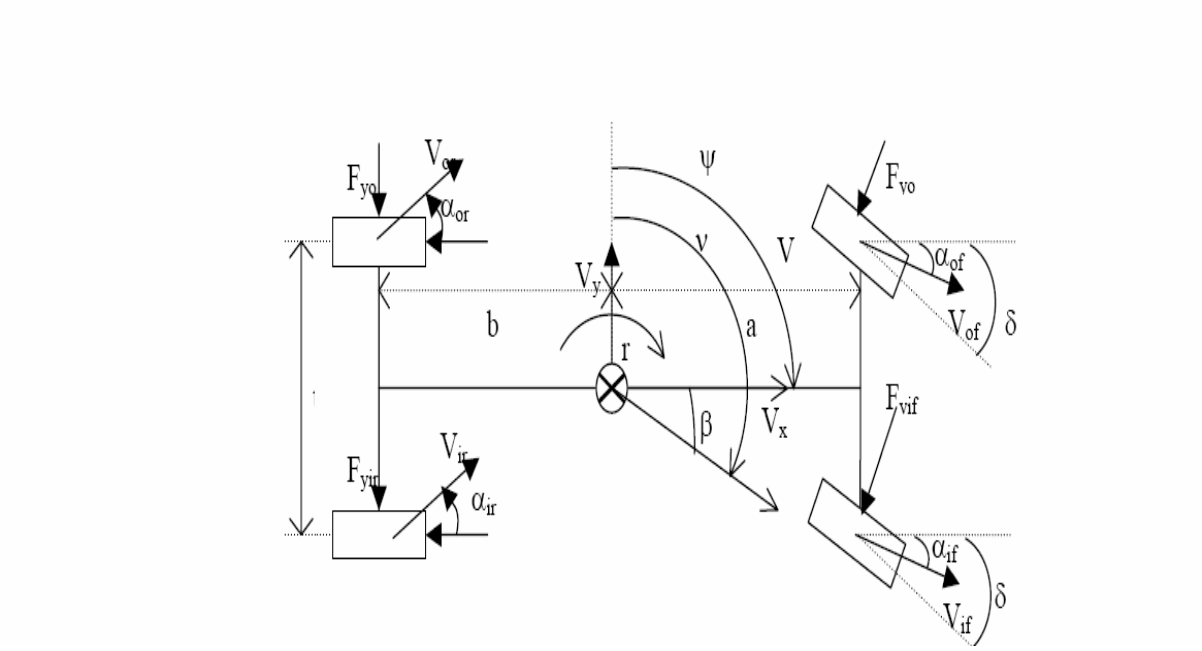


**Figure 3.3: Four Wheel Vehicle Schematic Showing the Full Lateral Dynamics of a Vehicle**

In the figure (3.3) the lateral dynamics of the vehicle are derived by summing the forces and the moments about the center of gravity of the vehicle as shown below.

$$\sum F_y = ma_y = (F_{yor} + F_{yir}) + (F_{yof} + F_{yif})\cos(\delta)$$

$$\sum M_{cg} = I_z \ddot{\psi} = -b(F_{yor} + F_{yir}) + a[(F_{yof} + F_{yif})\cos(\delta)] + t/2[(F_{yof} - F_{yif})\sin(\delta)] \ldots (3.1)$$

Where V is the heading velocity

$$a_y = (V_r + \dot{V}_y) = [V_r + \dot{V}\sin(\beta) + V\dot{\beta}\cos(\beta)]$$

$$\ddot{\psi} = \dot{r}$$

By solving the above equations for $\dot{\beta}$ & $\dot{r}$ , the equations of motion for the

vehicles lateral dynamics can be found and are shown in Equation (3.2)

$$\dot{\beta} = \frac{(F_{yor} + F_{yir}) + (F_{yof} + F_{yif})\cos(\delta)}{mV\cos(\beta)} - r - \frac{\dot{V}\tan(\beta)}{V} \quad \text{.....(3.2)}$$

$$\dot{r} = \frac{-b(F_{yor} + F_{yir}) + a[(F_{yof} + F_{yif})\cos(\delta) + t/2[(F_{yof} - F_{yif})\sin(\delta)]}{I_z}$$

The tire slip angle ( α), as seen in Figure 3.3, is the difference between the tire's Longitudinal axis and the tire's velocity vector. The tire velocity vector can be found by Knowing the vehicle's velocity (at the center of gravity) and yaw rate. The direction or heading of the rear tire is the same as the vehicle heading, while the heading of the front tires must include the steer angle. The equation of the tire slip angles for all four tires is given in Equation (3)

$$\alpha_{if} = \tan^{-1}\left(\frac{V\sin(\beta) + ar}{V\cos(\beta) - \frac{t}{2}r}\right) - \delta$$

$$\alpha_{of} = \tan^{-1}\left(\frac{V\sin(\beta) + ar}{V\cos(\beta) + \frac{t}{2}r}\right) - \delta \qquad (3.3)$$

$$\alpha_{ir} = \tan^{-1}\left(\frac{V\sin(\beta) + ar}{V\cos(\beta) - \frac{t}{2}r}\right)$$

$$\alpha_{or} = \tan^{-1}\left(\frac{V\sin(\beta) + ar}{V\cos(\beta) + \frac{t}{2}r}\right)$$

The roll angle ( φ) of the vehicle is the amount of rotation of the vehicles sprung mass about its roll axis. In reality, the roll center of the vehicle does not remain constant, however for this thesis a stationary roll center is assumed in order to simplify the model. Some assumptions about the non-linear model of the vehicle can be made in order to linearize and simplify the model. One approximation used is to neglect weight transfer. This assumption causes the vertical forces at the tires to be equal to the static weights, which are the same on the left and right side of the vehicle. The next assumption made is that the tire slip angles ($\alpha$) are the same on the inner and outer sides of the vehicle.

Also, the inner and outer tires are assumed to be the same. Assuming the same inner and outer tires results in the tire cornering stiffness ($C_\alpha$) being the same for the inner and outer tires of the vehicle. Assuming no weight transfer, the same tire cornering stiffness (for the inner and outer tires), and the same tire slip angles (for the inner and outer tires) results in the lateral forces being equal for both the inner and the outer tire. Additionally, the vehicle's forward velocity is assumed to be constant in order to remove the acceleration term from the equations of motion. Finally, the small angle approximation is used in order to remove the trig metric terms from the equations of motion. These assumption simplify the vehicle model to what is commonly known as the bicycle model

shown in Figure 3.4. It is known as the bicycle model because the inner and outer dynamics are approximated as equal and therefore collapsed into two wheels.

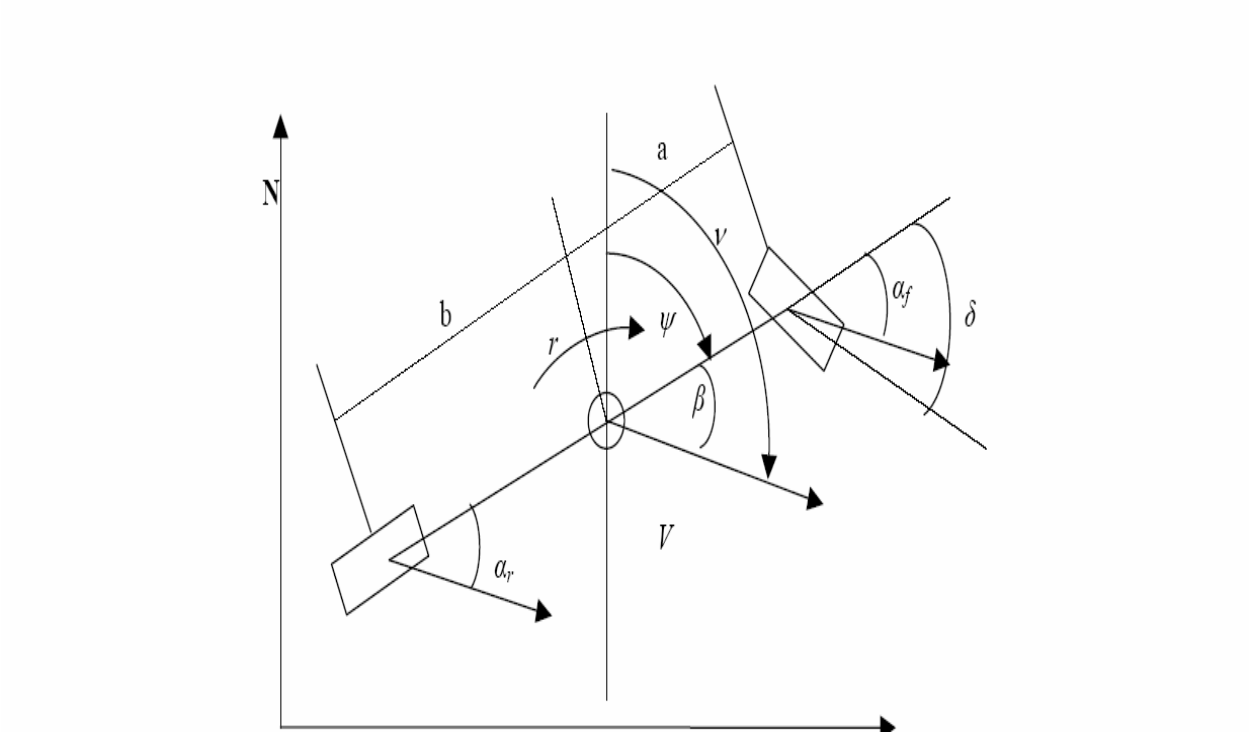


**Figure 3.4: Two wheel Bicycle Model Schematic of a Vehicle**

The non linear bicycle model considers longitudinal (x), lateral (y) ,yaw ( $\psi$ ) motion under the assumption of negligible lateral weight shift ,roll and compliance steer while traveling on a smooth road .Angular velocities of the front and rear tires are added to the states in order to investigate , directional interactions between longitudinal and lateral tire forces . In addition to these five states, longitudinal

and lateral positions and yaw angle with respect to the fixed inertial coordinates are added to the dynamic equation in order to refresh the vehicle position and orientation in the simulation scene. The bicycle model used in this simulator has five degrees of freedom with eight sate equations.

The equations of motion for the lateral dynamics of the simplified model are found the same way as the non-linear model (i.e. by summing the forces and moments around the center of gravity). This leads to the equation of motion for the bicycle model shown below in Equation (3.4).Note that in Equation (3.4), $C_{\alpha f}$ and $C_{\alpha r}$ are the tire cornering stiffness for the front and rear axle, respectively.

$$\sum F_y = F_{yf} + F_{yr} = ma_y = m(V\dot{\beta} + Vr)$$

$$\sum M_y = aF_{yf} - bF_{yr} = I_z\dot{r}$$

Where

$$F_{yf} = C_{\alpha f}\alpha_f \approx C_{\alpha f}\left(\beta + \frac{ar}{V}\right) - \delta \quad \textbf{.....(3.4)}$$

$$F_{yr} = C_{\alpha r}\alpha_r \approx C_{\alpha r}\left(\beta - \frac{br}{V}\right)$$

The above linear equations of motion can be rewritten in the state space form show in Equation (3.5).

$$\dot{X} = AX + Bu \text{ ……..(3.5)}$$

$$Y = CX$$

Where X= States

Y=Measurements

U= Input

A= State matrix

B=Input matrix

C=Output matrix

the equations for steady state yaw rate and steady state sideslip can be derived

$$r_{ss} = \frac{V}{L + V^2 K_{us}} \delta$$

The under steer gradient ($K_{us}$) defines whether the vehicle is under steer ($K_{us}<0$), over steer ($K_{us}>0$), or neutral steer ($K_{us}=0$).

The simulations were performed on the model with parameters as

m=1340kg, $I_x = 2910\,\text{kg}.m^2$, $I_f = 1.22m, I_r = 1.62m$ and $C_{\alpha f} = C\alpha_r = 2 * 60000N/rad$

$K_{us}$ = 4.1071 (deg/g), a = 1.2048m, b = 1.3862 m.

Equations (3.1) (3.2) (3.3) (3.4) were simulated and the following assumptions were taken into account, these equations were solved in matlab .

1) The vehicle is moving on a fixed horizontal frame
2) Vehicle is moving at a very low speed
3) Longitude slippage is neglected
4) Lateral force on the tire is directly proportional to the vehicle load
5) Wheel actuation is equal on each side in order to reduce the longitudinal slip
6) Vehicle is rotating in counterclockwise direction

The vehicle's lateral tire forces versus slip angle for the front and rear tires are shown in Figure 3.5

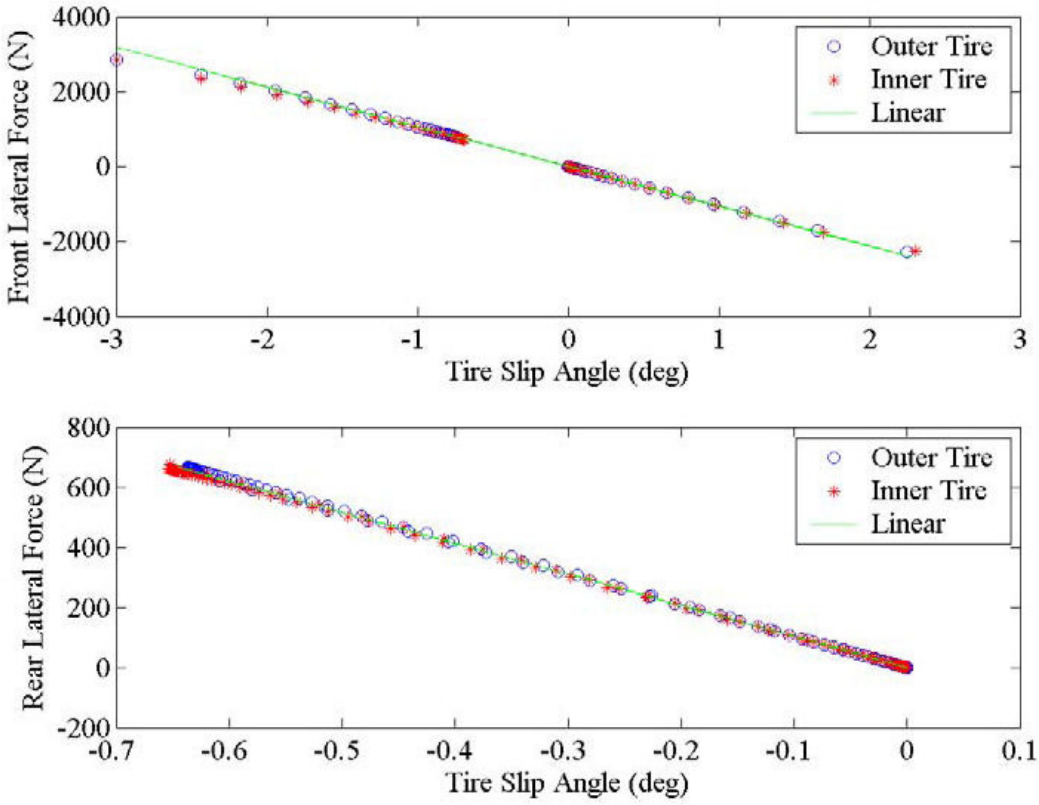


**Figure 3.5: Tire Forces for each Tire Front and Rear in Linear**

The vehicle's sideslip and yaw dynamics are shown for both the linear and nonlinear model in Figure 3.6. As expected, the vehicle's linear and non-linear models match each other since the tire cornering stiffness for linear model is close to the average of the two lateral forces for each tire.

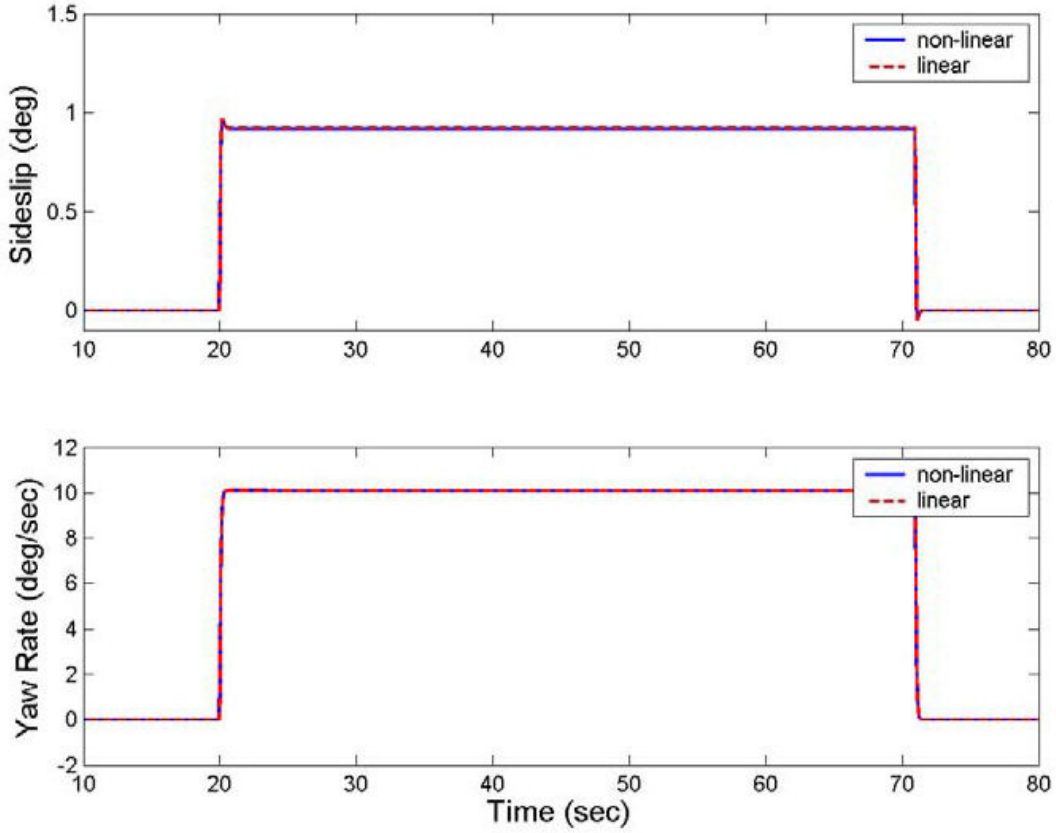


**Figure 3.6: States in the Linear Region for the Linear and Non-linear Models**

Next, the simulation was repeated for a high lateral acceleration maneuver. A step steer input was chosen to cause all four tires to enter the non-linear region of the tire curve. The tire cornering stiffness for the linear model of each axle was not corrected for the tires leaving the linear region of the tire curve. The inner and outer tire lateral force versus tire slip angle as well as the linear tire model for the front and rear axle of this Simulation is shown in Figure 3.7. This graph shows that all four tires operate in the nonlinear region of the tire curve. Note that the linear tire model uses the tire cornering stiffness when all four tires of the vehicle where in the linear tire region of the tire curve.

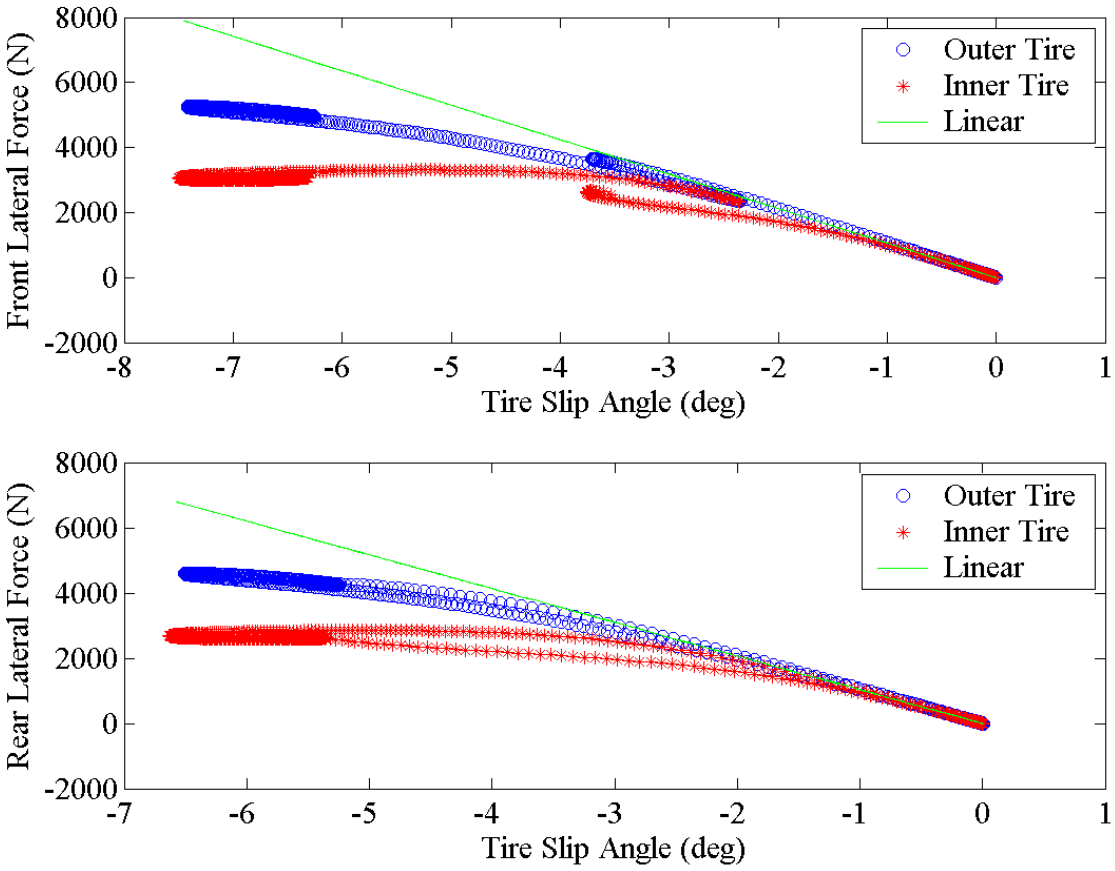


**Figure 3.7: Tire Forces for the High Lateral Acceleration Maneuver with Incorrect Tire Cornering Stiffness**

The sideslip and the yaw rate of the vehicle were recorded for both the linear and non-linear models and are shown in Figure 3.8. The errors in both sideslip and yaw rate are due to weight transfer and the non-linear tire characteristics. By the tires leaving the Linear region of the tire curve, the tire cornering stiffness for these tires has changed. The tire cornering stiffness is no longer the slope of the line in the linear region of the tire curve but the slope of the line tangent to the area where the vehicle is operating in the tire

curve

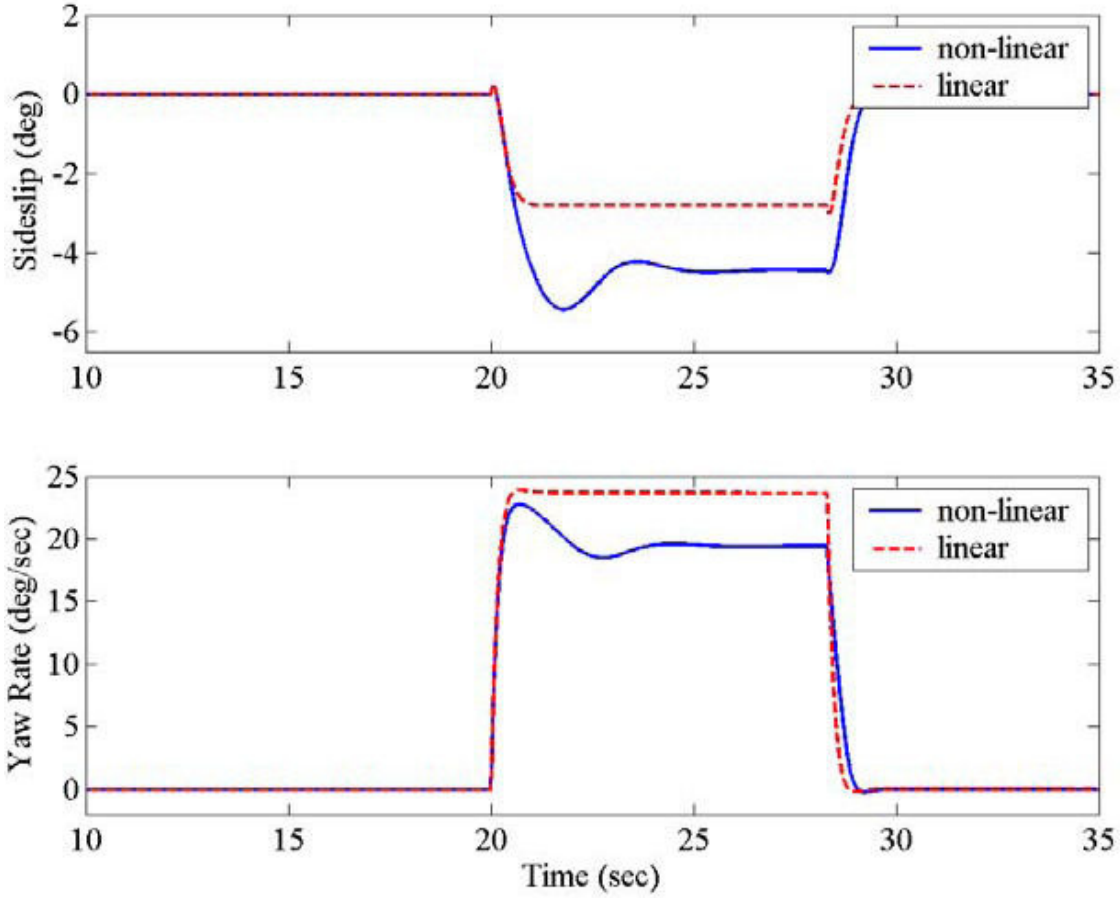


**Figure 3.8: States using Non-modified Linear Tire Cornering Stiffness With all Four Tires in the Non-linear Region**

The final simulation performed was again for the high lateral acceleration maneuver. However, this time the total front and rear tire cornering stiffness used in the linear model was modified (to account for the change of the tire cornering stiffness in the inner tires) to be the sum of the steady state lateral forces divided by the average slip angle for each axis. The equation for the modified front and rear tire cornering stiffness

is shown in Equation (3.6).

$$C_{\alpha f} = \frac{F_{yif} + F_{yof}}{\frac{\alpha_{if} + \alpha_{of}}{2}} \text{ .....(3.6)}$$

$$C_{\alpha r} = \frac{F_{yif} + F_{yof}}{\frac{\alpha_{if} + \alpha_{of}}{2}}$$

The lateral force versus slip angle for the simulation is again shown in Figure 3.9. The figure also shows the modified linear tire model used for this simulation. Note the change in the linear tire curve in Figure 3.9 from the linear tire curve in Figure 3.8. This is due to the fact that the front and rear tire cornering stiffness was modified to account for all four tires operating in the non-linear region of the tire curve. Note that the top portion of the curve in Figure 3.9 represents the steady state lateral tire force.

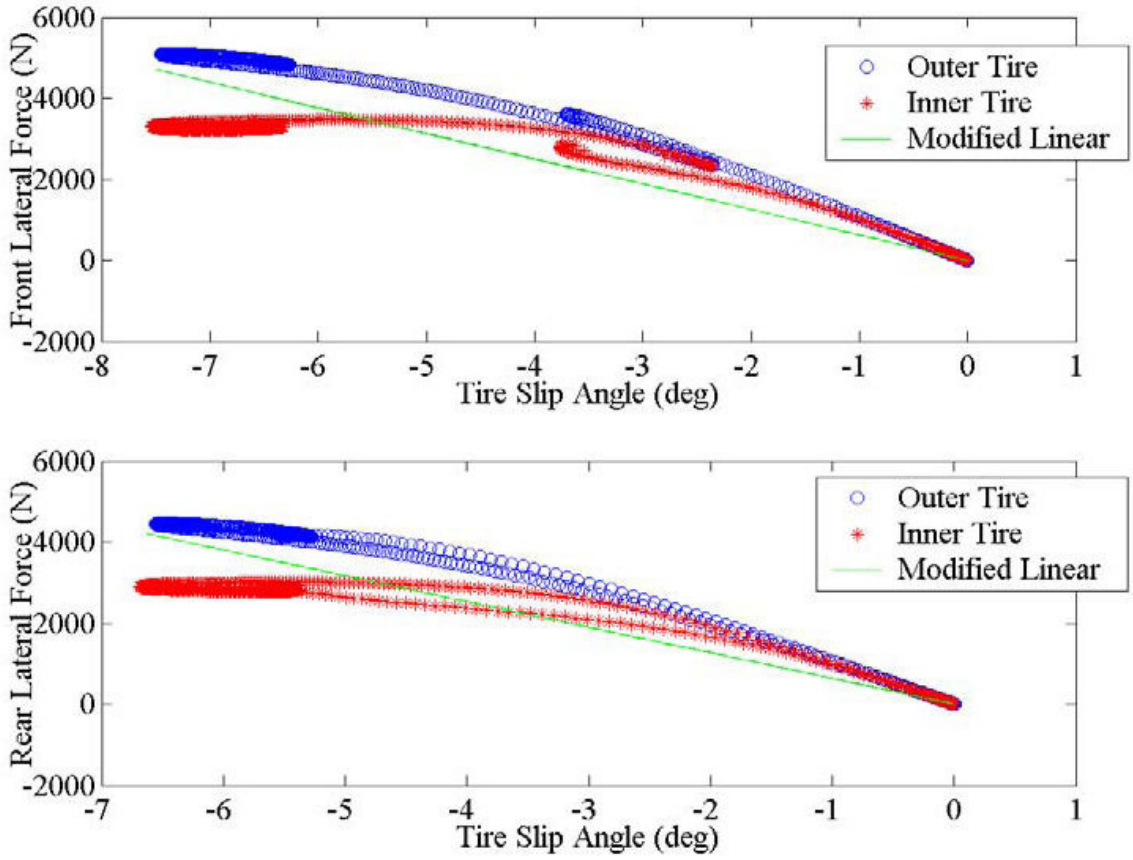


**Figure 3.9: Tire Forces for the High Lateral Acceleration Maneuver with Modified Linear Tire Cornering Stiffness**

**2.3 Effects of the road banked:**

Road bank angle has a direct influence on vehicle lateral and roll dynamics.Figure 3.10 provides a schematic of a vehicle on a banked turn.

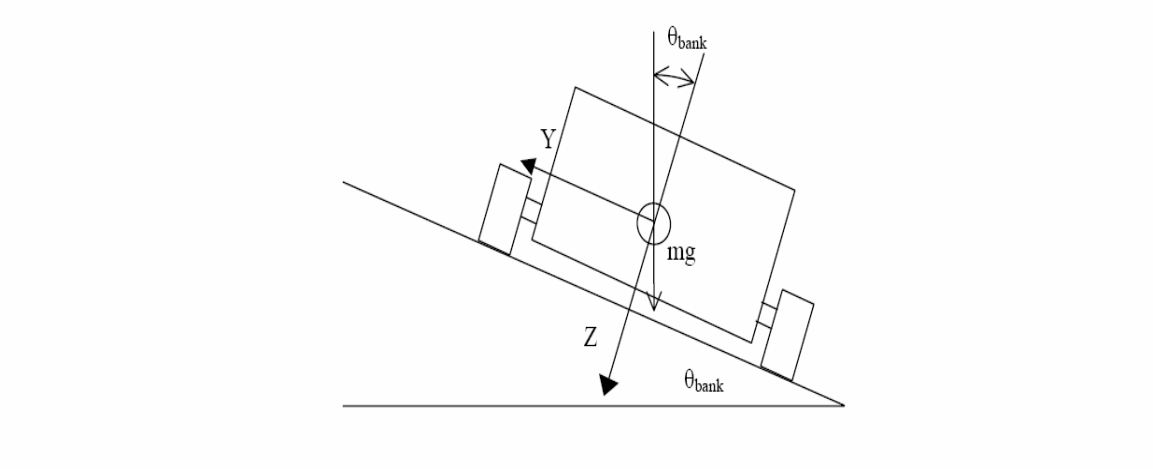


**Figure 3.10: Schematic of a Vehicle on a Banked Turn**

It can be seen in the figure that a component of the vehicle weight lies along the lateral axis and will have an effect on the lateral dynamics of the vehicle. Additionally, the bank angle will have an effect on the roll dynamics of the vehicle. In a normal banked turn, the bank will reduce the total roll of the vehicle. This is because the bank is going to cause the vehicle to roll in the opposite direction of the roll due to lateral acceleration. This can

be seen in Equation (3.7) where the lateral forces now include the effects of road bank (which are ignored in the linearized state space model shown in

$$\sum F_y = F_{yf} + F_{yr} = ma_y = m(V\dot{\beta} + Vr) - mg\sin(\theta_{bank}) \quad \text{.....(3.7)}$$

$$\sum M_y = aF_{yf} - bF_{yr} = I_z \dot{r}$$

Where V is the heading velocity

$$F_{yf} = C_{\alpha f}\alpha_f \approx C_{\alpha f}\left(\beta + \frac{ar}{V}\right) - \delta$$

$$F_{yr} = C_{\alpha r}\alpha_r \approx C_{\alpha r}\left(\beta - \frac{br}{V}\right)$$

Additionally, a simulation was performed in order to show the effects of a banked turn on the yaw dynamics. As was stated previously in this section, the road bank will require less steer angle while the vehicle yaw dynamics and sideslip angle will have little change.. The simulation used parameters of a model of a vehicle driving around two 180° constant radius turn with an eight degree bank.

In order to capture the effect of bank angle, the simulation was first performed using the steer angle of the vehicle on flat ground to get the sideslip angle and yaw rate of the vehicle. Next, a banked steer angle was formed by modeling the effects the road bank has on the steer angle of the vehicle in a steady state turn. The equation for the bank model can be seen in Equation (9).

$$mg\sin(\theta_{bank}) = C_{\alpha f}\delta_{off} \text{ ……..(3.8)}$$

$$\delta_{bank} = \delta_{flat} - \delta_{off}$$

These two steer angles for the simulation can be seen below in Figure 3.11. This figure contains the steer angle for a flat turn (needed to make the yaw rate and sideslip) and the steer angle due to a banked turn.

Equations (3.1) (3.2) (3.3) (3.4) (3.5) (3.6) (3.7) (3.8) were simulated in matlab and the following assumptions were taken into considerations.

1) The vehicle is moving on a fixed horizontal frame
2) Vehicle is moving at a very low speed
3) Longitude slippage is neglected
4) Lateral force on the tire is directly proportional to the vehicle load
5) Wheel actuation is equal on each side in order to reduce the longitudinal slip
6) Vehicle is rotating in counterclockwise direction

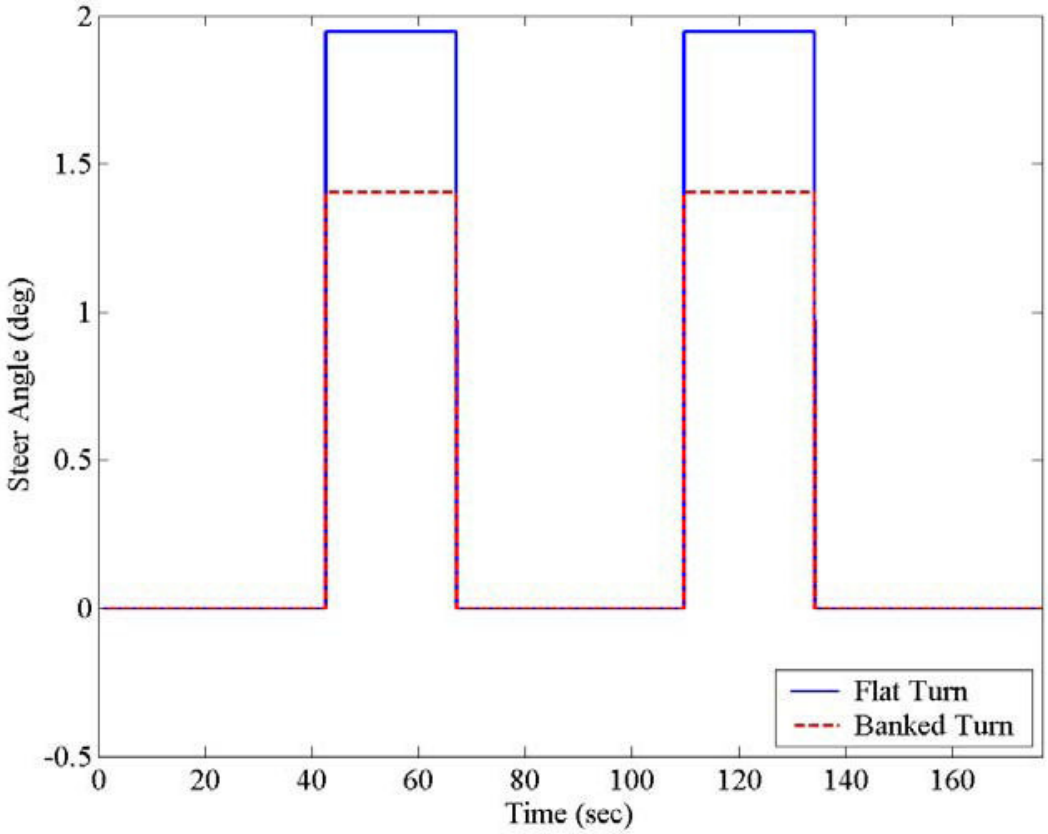


**Figure 3.11: Steer Angle for a Vehicle on a Flat and Banked Constant Radius Turn**

Additionally, Figure 3.12 shows the sideslip and yaw rate for both steer angles.

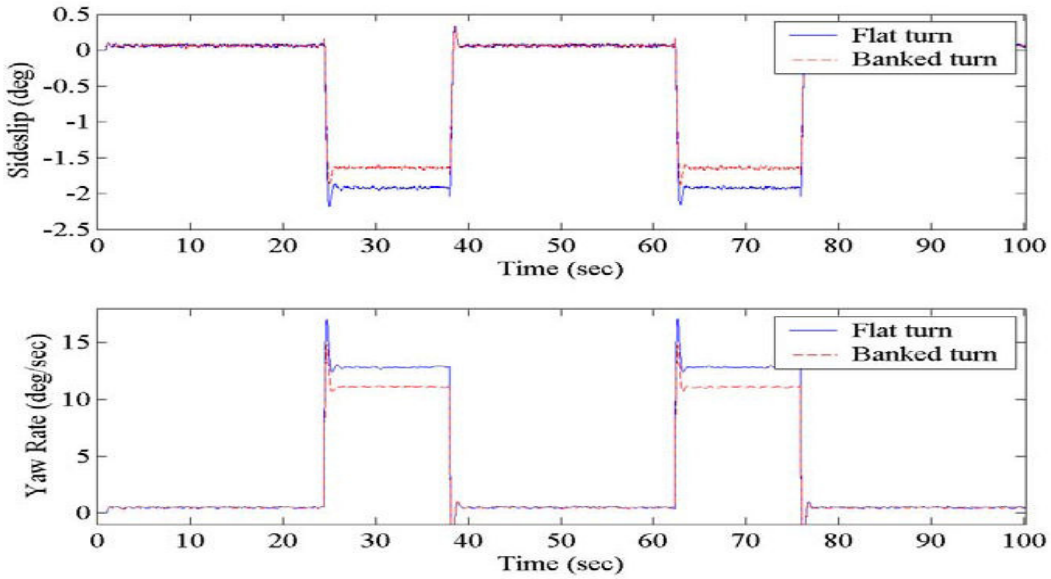


**Figure 3.12: Vehicle States for Different Steer Angle**

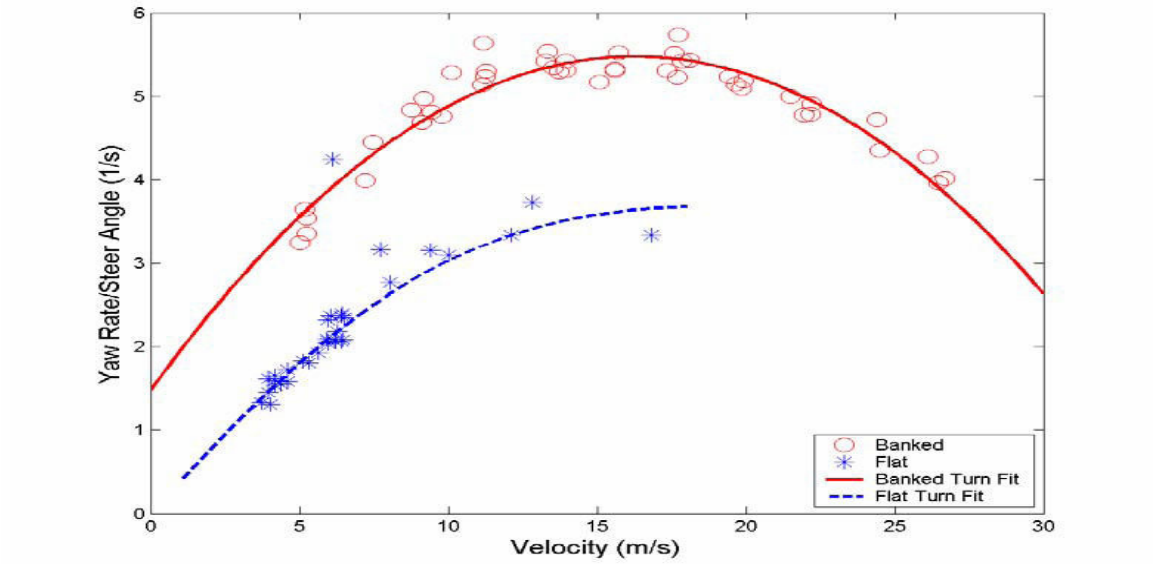


**Figure 3.13 Yaw rate Vs Velocity**

This chapter provided the basic model of the vehicle's lateral and roll dynamics. The model was linearized and simplified to form the bicycle model for the lateral dynamics. Additionally, this chapter has shown the non-linear tire model and shown its effects. Also, this chapter has shown the effects of road bank on the vehicles lateral dynamics.

# CHAPTER 4

# MATHEMATICAL MODELLING

This chapter discusses the mathematical model used for the vehicle. It has been separated into two main sections: Kinematics and Dynamic..

**4.1 Derivation of Kinematics Model :**

The first step taken in the derivation is to create the kinematics model by employing the nonholonomic constraints. These constraints hold under the assumption that there is no slippage at the wheel. A nonholonomic constraint is one that is not integrable. The constraints related to an automobile are those of the vehicle's velocity. As a result, the general form of the nonholonomic constraint

$$\dot{u}\sin(\theta) - \dot{\omega}\cos(\theta) = 0 \qquad (4.1)$$

Where $\dot{u}$ and $\dot{w}$ are the velocities of a wheel within a given (*u,w*) coordinate system, and $\theta$ is the angle of the wheel with respect to the x-axis. With this in mind, we examine a general front-wheel steer, rear-wheel drive vehicle. For small angles of steering, the XUV can be modeled as a bicycle, as shown in Figure 4.1.

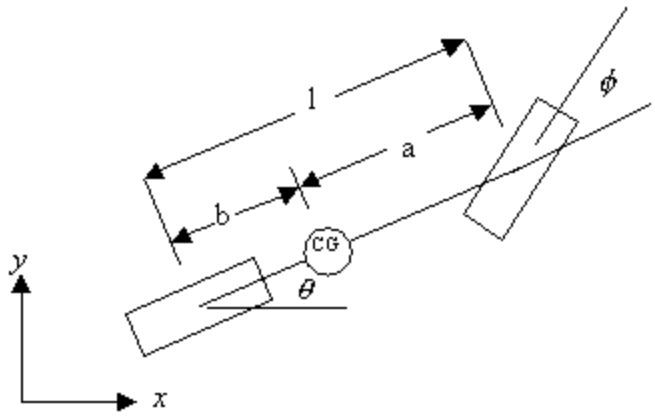


**Figure 4.1: General Coordinates of an XUV like of robot**

Denote (*x; y*) as being the position of the center of gravity, $\theta$ as the orientation of the vehicle with respect to the x-axis, and $\phi$ as the steering angle between the front wheel and the body axis. Let (*x*1*; y*1) denote the position of the rear axle, and (*x*2*; y*2) denote the position of the front axle. This defines,

$$x_1 = x - b\cos(\theta), x_2 = x + a\cos(\theta) \tag{4.2}$$

$$y_1 = y - b\sin(\theta), y_2 = y + a\sin(\theta) \tag{4.3}$$

$$\dot{x_1} = \dot{x} + b\dot{\theta}\sin(\theta),\ \dot{x_2} = \dot{x} - a\dot{\theta}\sin(\theta) \tag{4.4}$$

$$\dot{y_1} = \dot{y} - b\dot{\theta}\cos(\theta),\ \dot{y_2} = \dot{y} + a\dot{\theta}\cos(\theta), \tag{4.5}$$

The nonholonomic constraints are then written for each wheel, resulting in

$$\dot{x}_1 \sin(\theta) - \dot{y}_1 \cos(\theta) = 0, \tag{4.6}$$

$$\dot{x}_2 \sin(\theta + \phi) - \dot{y}_2 \cos(\theta + \phi) = 0, \tag{4.7}$$

Substituting the definition of $(\dot{x}_1, \dot{y}_1)$ and $(\dot{x}_2, \dot{y}_2)$ into equation (4.6) and (4.7) gives

$$\dot{x}\sin(\theta) - \dot{y}\cos(\theta) + b\dot{\theta} = 0, \tag{4.8}$$

$$\dot{x}\sin(\theta + \phi) - \dot{y}\cos(\theta + \phi) - a\dot{\theta}\cos(\phi) = 0, \tag{4.9}$$

Using the coordinate frame of the vehicle, as shown in Figure 4.2, define the *u*-axis as being that which is along the length of the vehicle and the *w*-axis normal to the *u*-axis,

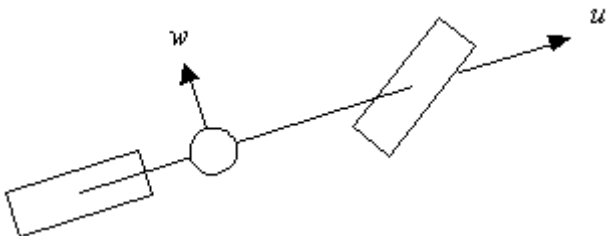


**Figure 4.2: Robotic Vehicle body coordinates**

Define :

$$\dot{x} = v_u \cos(\theta) - v_w \sin(\theta), \tag{4.10}$$

$$\dot{y} = v_u \sin(\theta) + v_w \cos(\theta), \tag{4.11}$$

Where *vu* and *vw* are the velocities of the center of gravity along the *u* and *w* axes, respectively. Substituting these definitions into equations (4.10) and (4.11) results with

$$v_w = \dot{\theta} b \tag{4.12}$$

$$\dot{\theta} = \frac{\tan\phi}{l} v_u \tag{4.13}$$

Thus, the derivatives of the nonholonomic equations are

$$\dot{v}_w = \ddot{\theta} b \tag{4.14}$$

$$\dot{\theta} = \frac{\tan\phi}{l} v_u + \frac{v_u}{l(\cos\phi)^2} \dot{\phi} \tag{4.15}$$

**4.2 Derivation of dynamic model**

Now that the kinematics constraints are in a more useful format, the dynamic equations can be derived. These dynamic equations are similar to those found in chapter 3, with a couple added assumptions. These added assumptions are that there is no friction force between the wheels and the vehicle, and that the rear wheels are locked to be in the same

Orientation as the vehicle. Other assumptions used both in chapter 3 and this paper is that there is no slip at the wheel, and that the driving force, based on the radius of the wheel and the drive torque, can be modeled as acting at the center of the rear wheels. With the slippage assumption comes a pair of forces, one acting at each wheel, and perpendicular to that wheel. The forces involved in this derivation are shown in Figure 4.3.

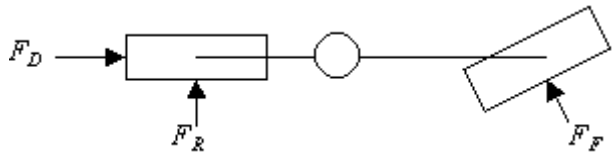


**Figure 4.3 Xuv input and resultant forces**

The resultant dynamic equations are

$$\dot{v}_u = v_w \dot{\theta} - \frac{F_F \sin(\phi)}{m} + \frac{F_D}{m} \tag{4.16}$$

$$\dot{v}_w = -v_u \dot{\theta} + \frac{F_F \cos(\phi)}{m} + \frac{F_R}{m} \tag{4.17}$$

$$\ddot{\theta} = \frac{aF_F \cos(\phi)}{j} - \frac{bF_R}{j} \tag{4.18}$$

Where $m$ and $J$ are the mass and mass moment of inertia of the vehicle about the center of

Gravity. $F_D$ is the driving force, applied at the rear axle, along the *u*-axis, and $F_F$ and $F_R$ are the resultant lateral forces on the front and rear tires respectively.

Solving equation (4.18) in terms of $F_R$ gives:

$$F_R = \frac{aF_F \cos(\phi)}{b} - \frac{J\ddot{\theta}}{b} \tag{4.19}$$

Substituting equations (4.14) and (4.19) into equation (4.17) reveals:

$$\ddot{\theta} b = -v_u \dot{\theta} + \frac{F_F \cos(\phi)}{m} + \frac{aF_F \cos(\phi)}{bm} - \frac{J\ddot{\theta}}{bm} \tag{4.20}$$

Solving equation (4.20) or $F_F$ gives :

$$F_F = \frac{b^2 m + J}{l\cos(\phi)}\ddot{\theta} + \frac{bm}{l\cos(\phi)} v_u \dot{\theta} \tag{4.21}$$

Placing equations (4.12) (4.13) (4.15) and (4.21) into equation (4.16) gives:

$$\dot{v}_u = \frac{v_u (b^2 m + J)\tan(\phi)}{\gamma}\dot{\phi} + \frac{l^2 (\cos\phi)^2}{\gamma} F_D \tag{4.22}$$

$$\gamma = (\cos\phi)^2 [l^2 m + (b^2 m + J)(\tan\phi)^2] \tag{4.23}$$

Placing equations (4.12) and (4.13) into the definitions of velocity and choosing states to be

X=[x y $\theta$ $v_u$ $F_D$ $\phi$ ]"

$$\dot{x} = [\cos\theta - \frac{b\tan\phi}{l}\sin\theta]v_u \tag{4.24}$$

$$\dot{y} = [\sin\theta + \frac{b\tan\phi}{l}\cos\theta]v_u \tag{4.25}$$

$$\dot{\theta} = \frac{\tan\phi}{l}v_u \tag{4.26}$$

$$\dot{v}_u = \frac{v_u(b^2m + J)\tan\phi}{\gamma}\dot{\phi} + \frac{l^2(\cos\phi)^2}{\gamma}F_D \tag{4.27}$$

$$\dot{F}_D = f(F_D, v_u, u_1) \tag{4.28}$$

$$\dot{\phi} = f(\phi, u_2) \tag{4.29}$$

Where $\gamma$ is defined by equation (4.23) and $u1$ and $u2$ are the input voltages, ranging from -5Vto 5V. The final step in deriving the dynamics of the system is to find equations for the driving force and the steering servo. The XUV is driven by diesel engine and hydraulic systems, but in these simulations it is considered if XUV is driven by Steering Servo motors then in order to do that the driving force is transmitted to the vehicle through an armature-controlled DC motor, the assumed model is derived as follows. The following equations of motion are related to steering Servo which is considered to be the prime moving element for XUV.

$$T_m = K_m I_a, I_a = \frac{u_1 - K_b w}{R_a + L_a s}$$

$$T_m = J_m \dot{w} + b_m w + T_D$$

$$K_m \frac{u_1 - K_b w}{R_a + L_a s} = J_m \dot{w} + b_m w + T_D \tag{4.30}$$

Where $K_m, K_b, R_b, L_a, J_m, and b_m$ all motor constants, w are is the angular velocity of the motor, and $T_D$ is the driving torque. Solving equation (4.30) for the driving torque and ignoring the higher order terms, which are three orders or magnitudes less or smaller, yields

$$\dot{T}_D = -\frac{R_a}{l_a} T_D - \frac{(K_m K_b + R_a b_m)}{l_a} w + \frac{K_m}{L_a} u_1 \tag{4.31}$$

Solving $T_D$ and w in terms of $F_D$ and $v_u$ gives :

$$T_D = \frac{N_m R_w}{N_w} F_{D,} w = \frac{N_w}{N_m R_w} v_u$$

$$\dot{F}_D = -\frac{R_a}{L_a} F_D - \frac{(K_m K_b + R_a b_m) N^2 w}{L_a N_m{}^2 R_w{}^2} v_u + \frac{K_m N_w}{L_a N_m R_w} u_1 \tag{4.32}$$

Where $R_w$ is the radius of the wheel and $N_w$ and $N_m$ are the number if teeth on the gears connecting the axle and motor respectively. The controller was assumed and experimentally proven, to be well represented by a linear first order system of the form.

$$\dot{\phi} = \frac{1}{\tau_s}\phi + c_s u_2 \tag{4.33}$$

In equation 4.33 $c_s$ is the Curvature of the Path on which the XUV is moving. Equation 4.33 is a state equation .

With equations (4.32) and (4.33), the full state equations can be re written as:

$$\dot{x} = [\cos\theta - \frac{b\tan\phi}{l}\sin\theta]v_u$$

$$\dot{y} = [\sin\theta + \frac{b\tan\phi}{l}\cos\theta]v_u$$

$$\dot{\theta} = \frac{\tan\phi}{l}v_u \tag{4.34}$$

$$\dot{v}_u = \frac{v_u(b^2m + J)\tan\phi}{\lambda}\dot{\phi} + \frac{l^2(\cos\phi)^2}{\gamma}F_D$$

$$\dot{F}_D = -\frac{R_a}{L_a} F_D - \frac{(K_m K_b + R_a b_m) N^2 w}{L_a N_m{}^2 R_w{}^2} v_u + \frac{K_m N_w}{L_a N_m R_w} u_1$$

$$\dot{\phi} = \frac{1}{\tau_s} \phi + c_s u_2$$

$\tau_s$ is the sampling time constant

**4.3 Simulation Results:**

In these simulation results a simple controller was modeled using the above dynamic equations of motion and the equations of electric motor which in this case is considered as the prime means of motion of XUV in order to modulate the speeds , then in the later section the effect of sampling time on the response of the vehicle is studied. This controller was designed to take the dynamics of the system into account .This controller was designed to check the behavior of the XUV vehicle in order to know the velocity response of the vehicle and to differentiate between the kinematics and dynamic response of the vehicle .

Parameters for controller for XUV taken into consideration are given below :

| | |
|---|---|
| L = Distance between rear wheel and front wheel in m | .254 |
| W = space between the wheels in m | .1651 |
| Height in m | 0.056 |
| Sampling time T in seconds | 0.01 |

The response of this controller is shown in Figures 4.4 and 4.5.

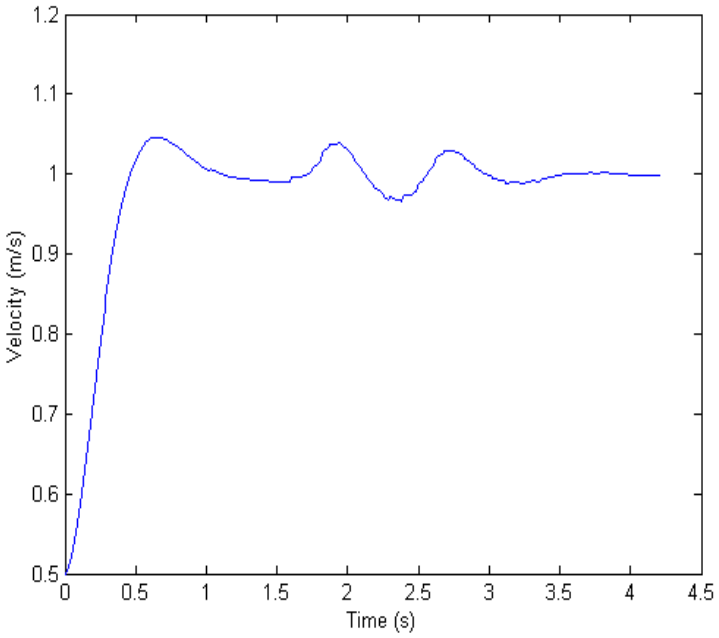


**Figure 4.4: Velocity response of XUV**

As shown by the figure 4.2 the settling time for velocity is half a second, further more the maximum overshoot is 4.6%.

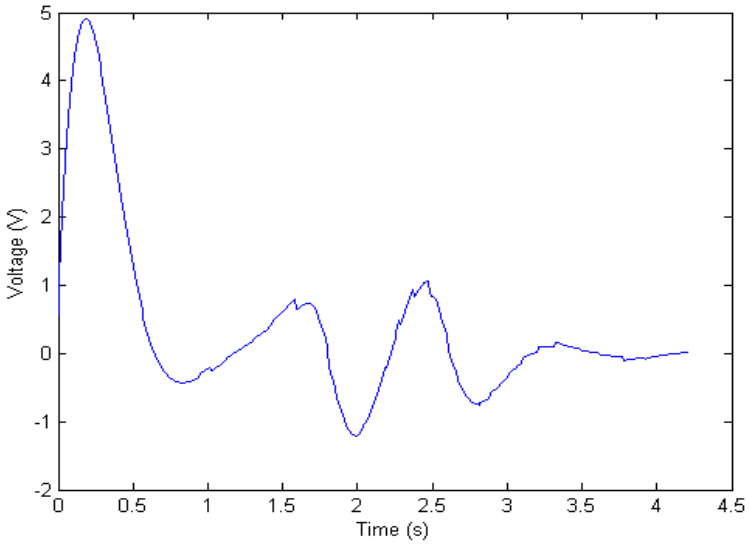


**Figure 4.5: Required control effort**

As shown in the figure 4.3, the voltage of the motor does not reach 5 volts, which means the controller is effectively controlling the vehicle.

### 4.3.1 Mathematical analysis:

. The effects of the servo dynamics have been shown to cause a significant change in the overall response of the vehicle. The next step is to explore when these dynamics have an effect and when they can be ignored. As a result, the simulation was run with the time constant of the servo $\tau_s$, ranging from 0.025,

half of the actual value, to 0.325 in steps of 0.050. As expected, the dynamic controller was virtually unaffected by the change in the servo response speed, Figures 4.6 and 4.15.

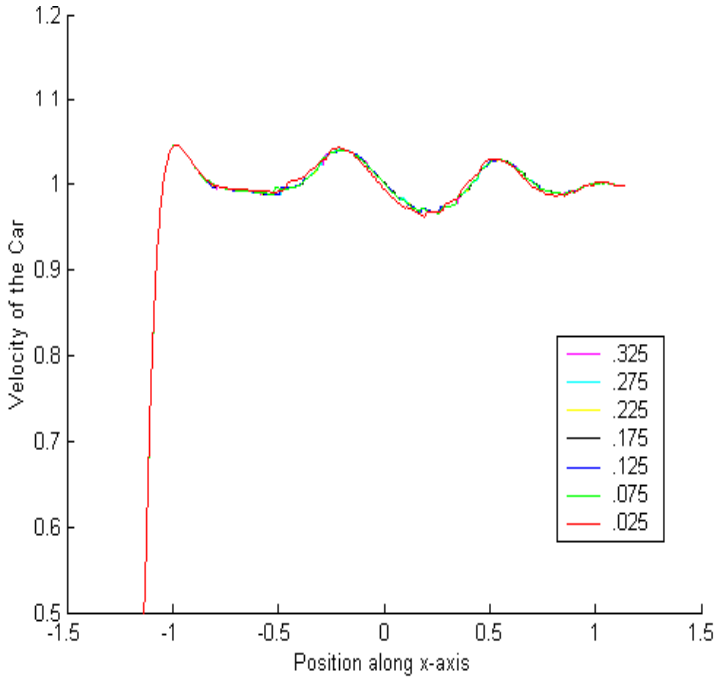


**Figure 4.6: Dynamic speed response w.r.t changing time constants**

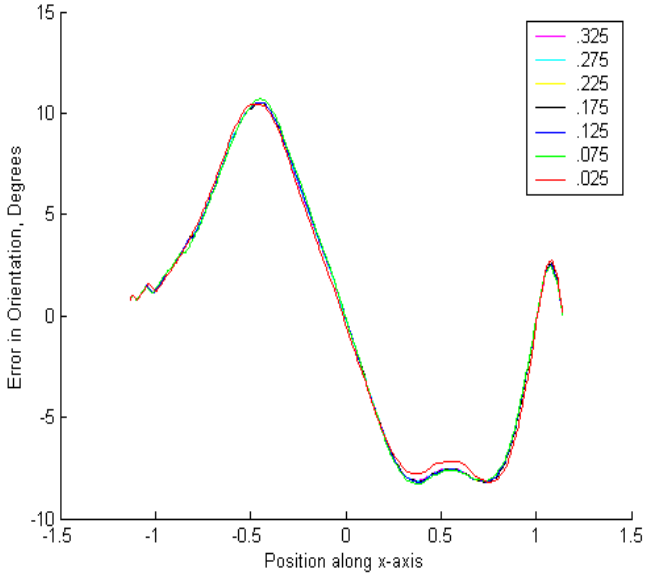


**Figure 4.7**: **Dynamic Error in Orientation w.r.t. Changing Time Constants**

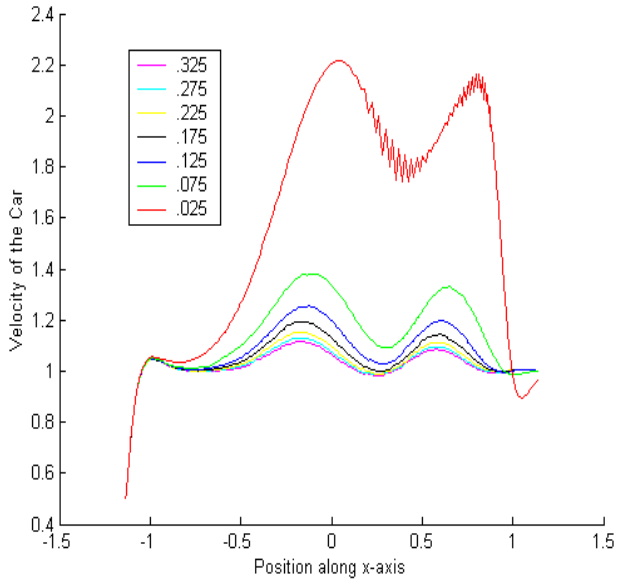


**Figure 4.8: Kinematics speed response w.r.t changing time constants**

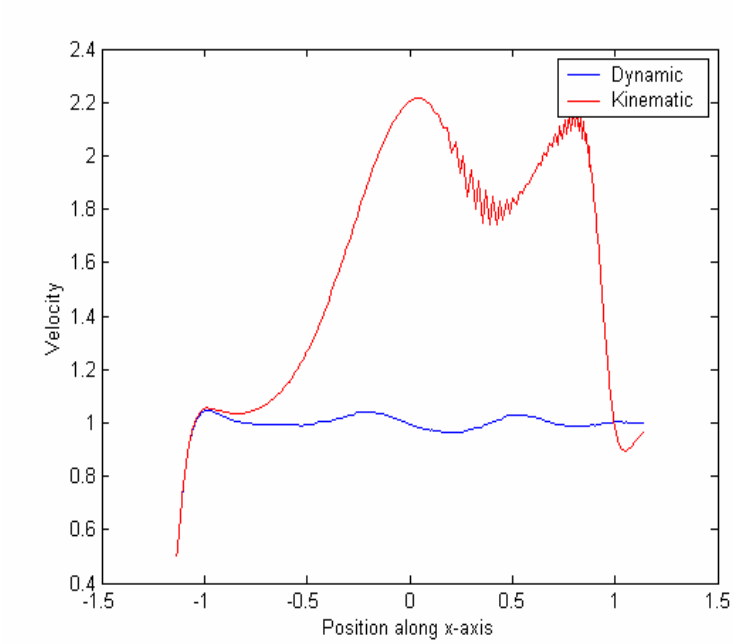


**Figure 4.9: Kinematics vs dynamic response in speed for $\tau_s = 0.025$**

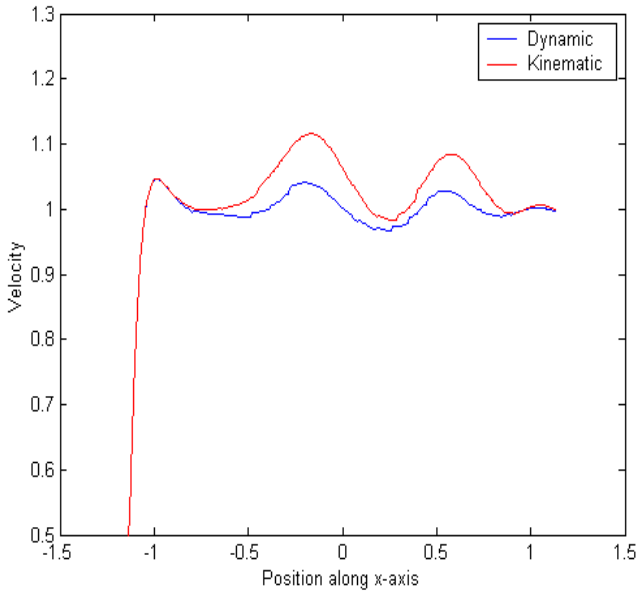


**Figure 4.10: Kinematics vs dynamic response in speed for $\tau_s = 0.325$**

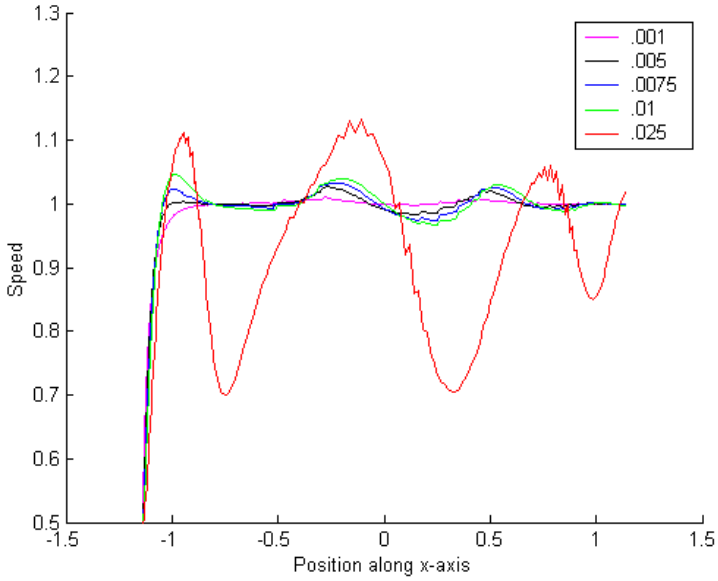


**Figure 4.10: Speed response w.r.t sampling period**

The kinematics controller which is used for speed modulation, on the other hand, showed some interesting results. The most notable is that, as the time constant for the servo increased, the amount of error decreased. Mathematically, this makes sense because as the time constant increases, it decreases the effect of the current state on the response. These results are shown in Figure 4.8. Furthermore, these plots show that, as the time constant increase, the kinematics response converges towards that of the dynamic response. This is made more clear when the kinematics and dynamic responses are plotted against each other for the time constants of $\tau_s$ = 0.025 and $\tau_s$ = 0.325. These plots can be seen in Figures 4.9, 4.10. It is worth mentioning that a time constant of 0.325 correlates to a settling time of roughly 1 second. The settling time for the servo used on the vehicle is on the order of 0.16 seconds. With this in mind, and the fact that the kinematics controller has yet to give a response equivalent to that of the dynamic controller, leads to the conclusion that including the dynamics of the servo is vital to a high quality controller and is not dismissible for any realistic values of $\tau_s$.There were other studies performed but we don't have theoretical results to compare with that , this assumption was made on the basis of the response received in the previous section .

**4.3.2: Side slip and yaw response simulation:**

In this simulation was performed on the XUV by using the equations of motion used in Chapter 3 ie equations 3.1, 3.2, 3.3, 3.4, 3.5, 3.6, 3.7, 3.8. Same assumptions were Taken into consideration and the simulations were performed in matlab .

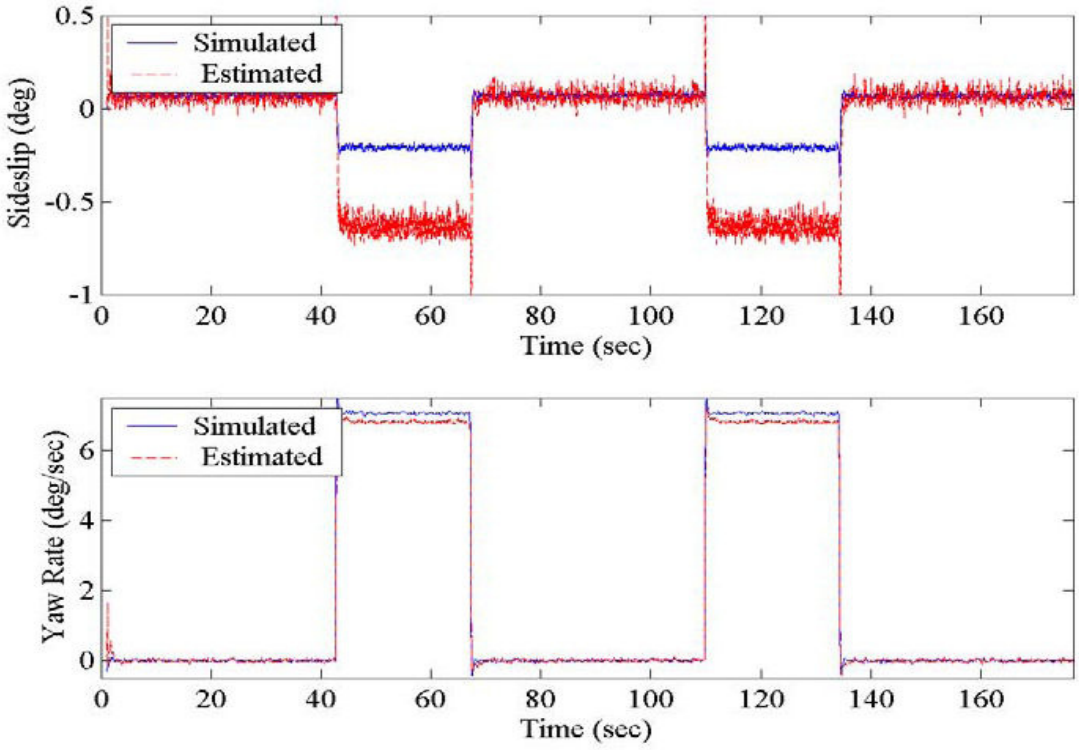


**Figure 4.11: Yaw rate and sideslip Vs time for a turn maneuver at 40 mph**

Figure 4.11 shows the yaw response and the side slip as the Xuv is maneuvered at 40 mph , the vehicle is turned on a 145 meter fixed radius turn with the same parameters of the vehicle as used in chapter 3 .The steer angle provide is 0.3 degree. The simulated and the estimated graphs shows that, the difference in the two curves are because of the errors associated in the graphs, Estimated graph is plotted when the kinematics and dynamic behavior of the vehicle is taken into account and the simulated is plotted when the dynamic parameters are taken into account , and the graphs are a little noisy because of the numerical errors.

In the next simulation the Xuv is maneuvered along a banked turn, the bank angle Applied is .5 degrees and the vehicle is going along a 145 meter turn at 40 mph, the Response is given by figure 4.12

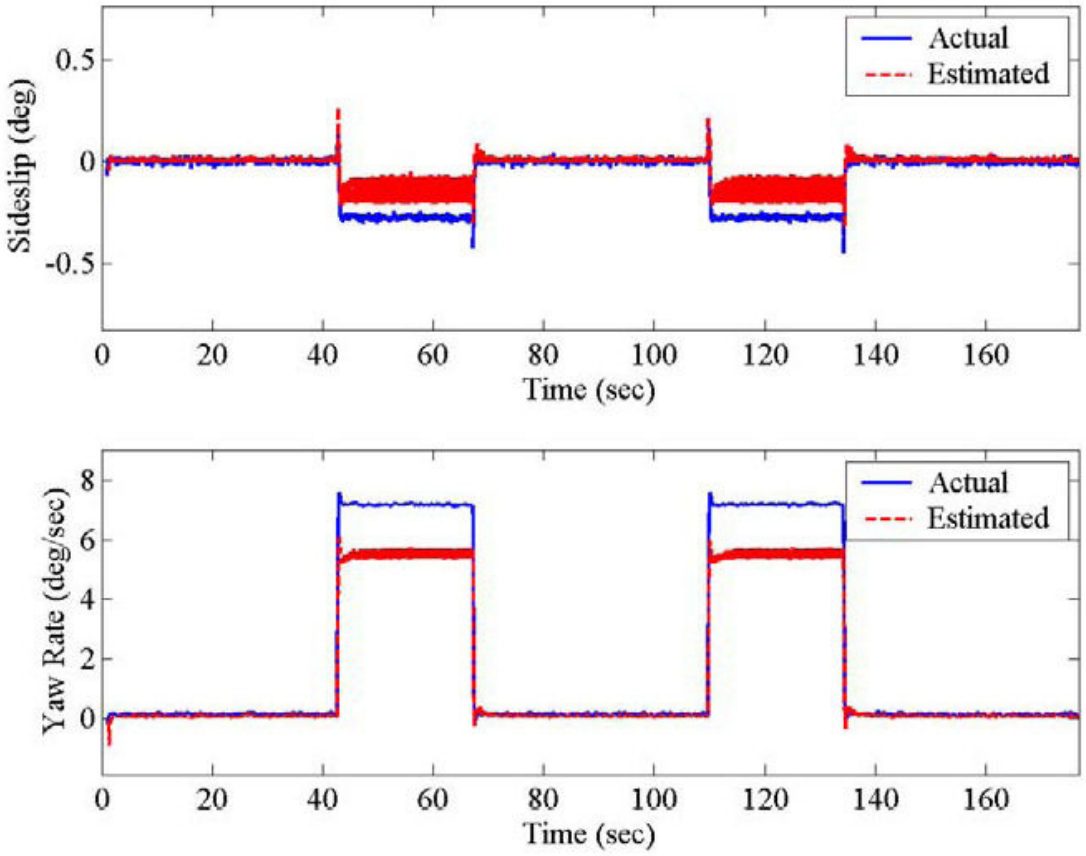


**Figure 4.13:** Yaw rate and sideslip Vs time for a turn maneuver at 40 mph Along a banked turn, bank angle = 0.5 degree

# CHAPTER 5

# XUV HANDLING BEHAVIOUR

This chapter includes the results obtained from matlab for different type of simulation performed on the XUV

**5.1 Dynamic simulations:**

The simulations were performed on the XUV with parameters as m=1340kg, $I_x = 2910\,\text{kg}.m^2$, $I_f = 1.22m, I_r = 1.62m$ and $C_f = C_r = 2 * 60000N/rad$. The cornering stiffness is increased by a factor of two since the tires at the back and front of the vehicle are lumped together.

The parameters used for the simulations on XUV in matlab are depicted in the table below:

**Table: 5.1: Parameters used for the Simulation of XUV using Matlab**

| Mass | $I_x$ | $I_f$ | $I_r$ | $C_f$ | $C_r$ |
|---|---|---|---|---|---|
| 1340 kg | 2910kg. $m^2$ | 1.22m | 1.62m | 60000N/rad | 60000N/rad |
| a(m) | b(m) | Length(m) | Track width | *Iz* | |
| 1.2048 | 1.3862 | 1.22 | 1.3840 | 3030 | |

\

Equations of motion taken into consideration were (3.1), (3.2), (3.3),(3.4), (3.5),(3.6),(3.7), (3.8) .

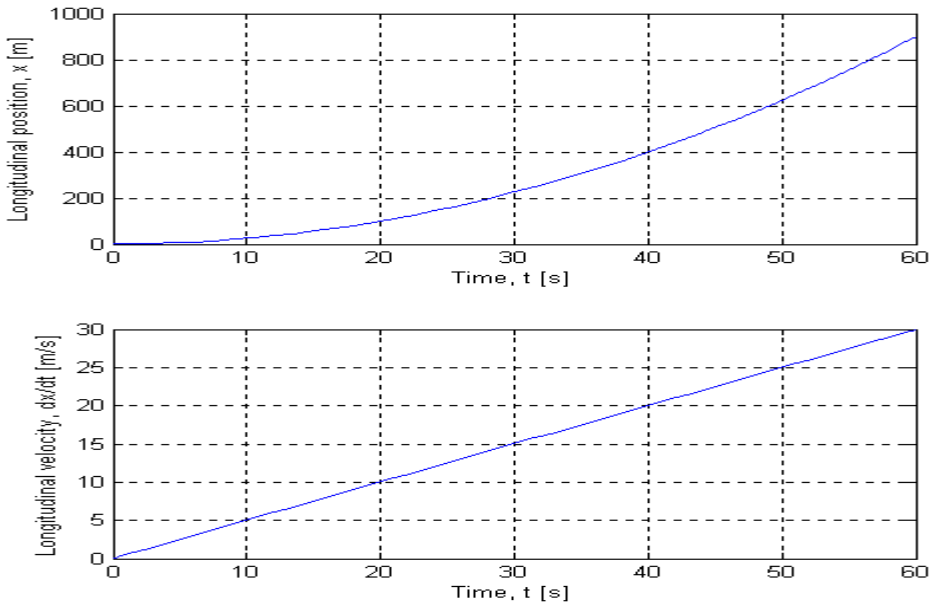


**Figure 5.1**: Constant Longitudinal acceleration

### 5.1.1 Constant longitudinal acceleration :

The first simulation set is a validation of the three-dimensional model for the longitudinal response of the vehicle. A constant acceleration of $u = 0.5m/s^2$ is applied to a vehicle initially at rest, i.e., with zero initial conditions, and no steering angle is applied, i.e. $\delta_f = 0$ ,

such that vehicle is accelerating in the longitudinal direction only. As shown in the plots given in Figure 4.6, the longitudinal position response is parabolic over time and the Longitudinal velocity response is linear. At t = 60s , the position x= 900 m and the velocity $V_x = 30m/s$ which match the expected results from a second-order, linear, longitudinal model under constant acceleration.

**5.1.2 Constant steering angle :**

In the second simulation set, a constant steering angle $\delta_f = 0.01rad$ is applied to a vehicle traveling with an initial velocity $V_0 = 25m/s$. For each simulation, the vehicle state responses are obtained and compared for various longitudinal acceleration inputs. Results for all six states and the vehicle trajectory are given in Figures 5.2 through 5.5

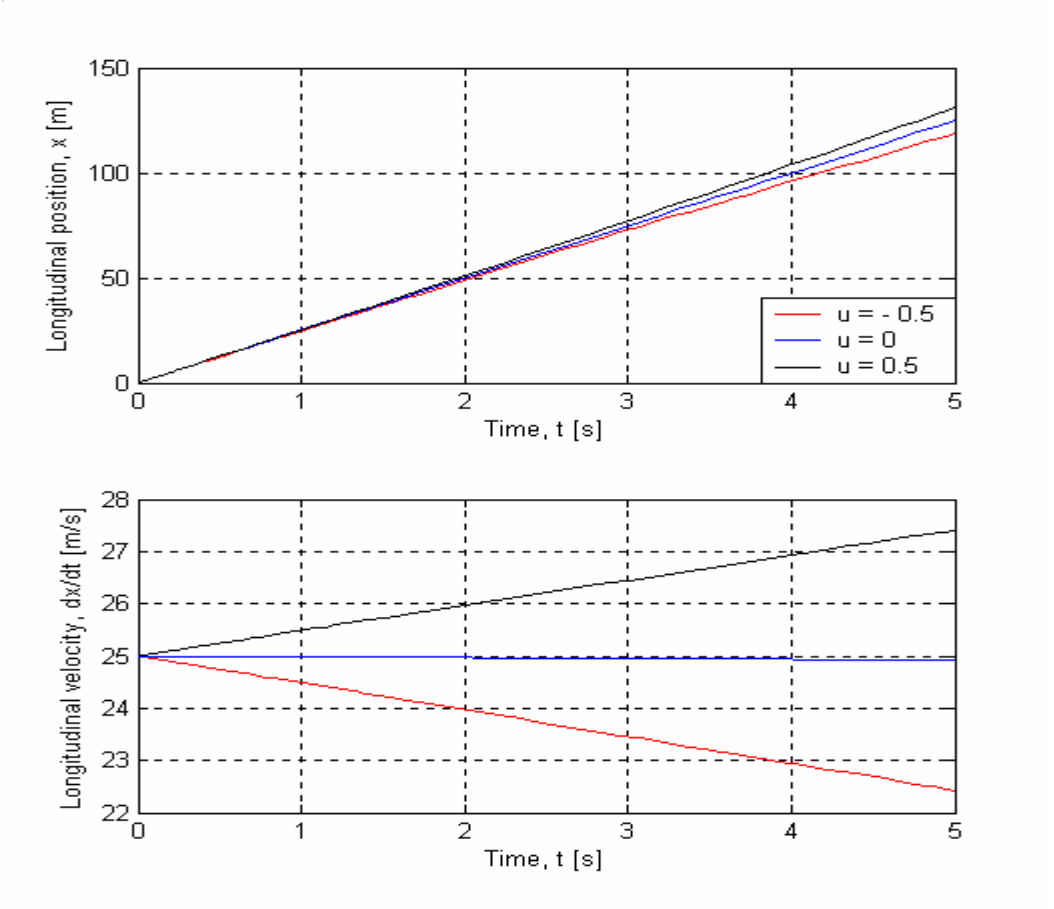


**Figure 5.2:** Longitudinal response for constant steering angle with initial velocity

From the plots given in Figure 5.2, the constant steering angle input results in a decrease in the longitudinal velocity. Indeed, for zero acceleration, the longitudinal velocity drops from its initial value of $V_0 = 25m/s$ , although this drop is rather negligible over the time span of 5 seconds. As shown in Figure 5.3, the vehicle responds quickly to a small steering input since the initial velocity is large. The vehicle begins by moving in the opposite direction of that desired as it first swerves in the positive y-direction for the initial 0.25seconds. The vehicle then moves in the negative y-direction, as desired. This phenomenon is due the initial cornering force on the tire, and for zero acceleration, the lateral velocity reaches a steady-state value of –0.12 m/s after 1 second. From the plots given in Figure 5.4, the yaw angle is roughly linear versus time for various longitudinal acceleration inputs. The first peak in the angular velocity response is consistent with the initial cornering force upon a steering input which causes a momentary rotation in the opposite direction. The lateral velocity reaches a steady-state value of 0.62 rad/s after 1 second. As shown in Figure 5.5, after 5 seconds, the vehicle has traveled a longitudinal distance of roughly 120 m. The difference in lateral position between positive and negative acceleration is small, less than 0.3 m after 5 seconds, but increasing

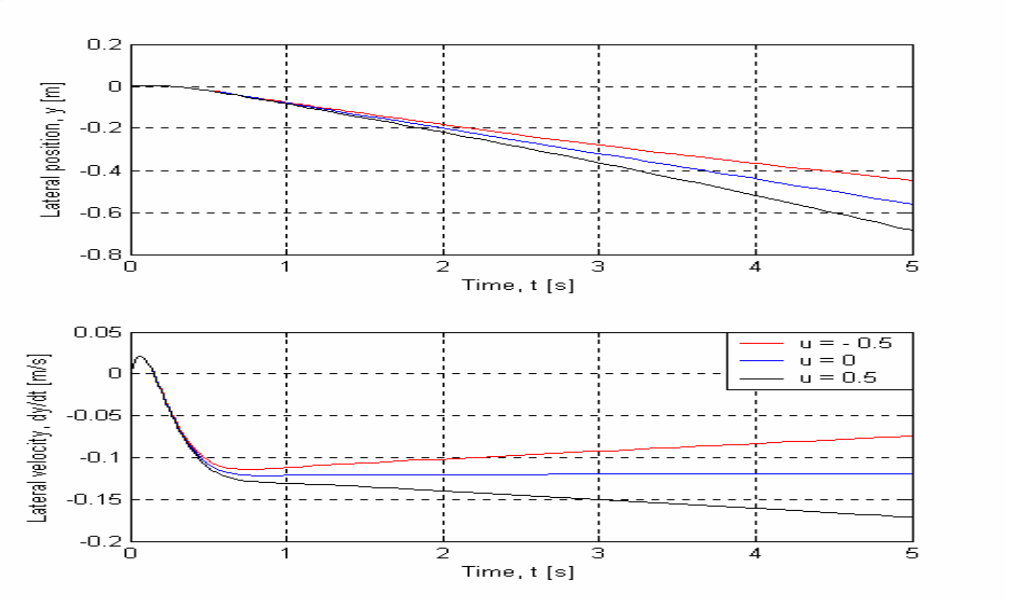


**Figure 5.3:** Lateral response for constant steering angle with initial velocity

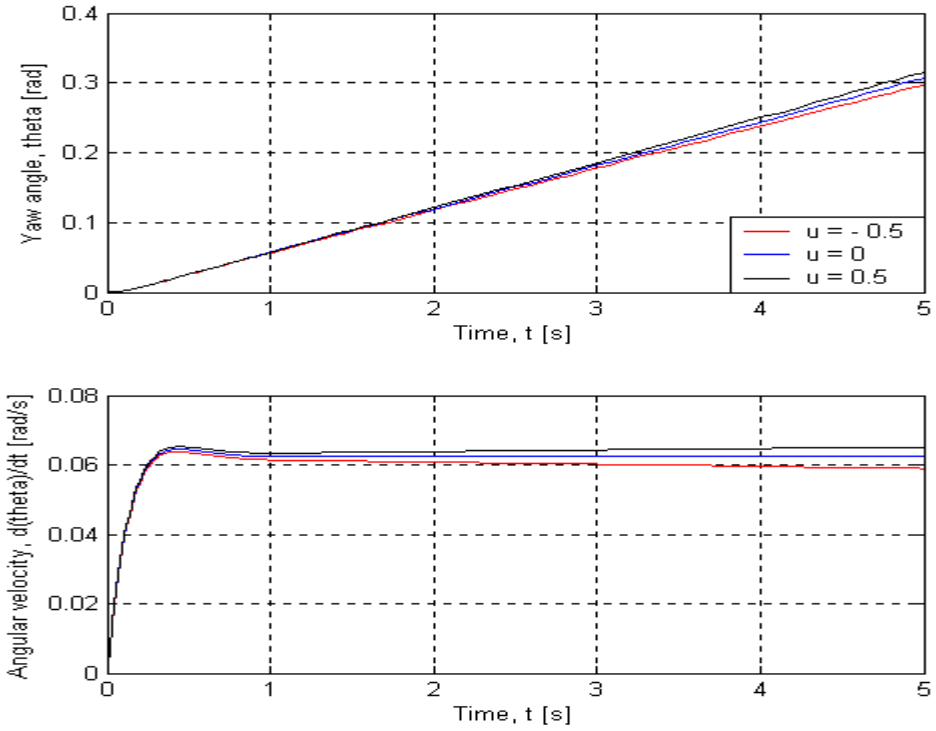


**Figure 5.4:** Angular response for constant steering angle with initial velocity

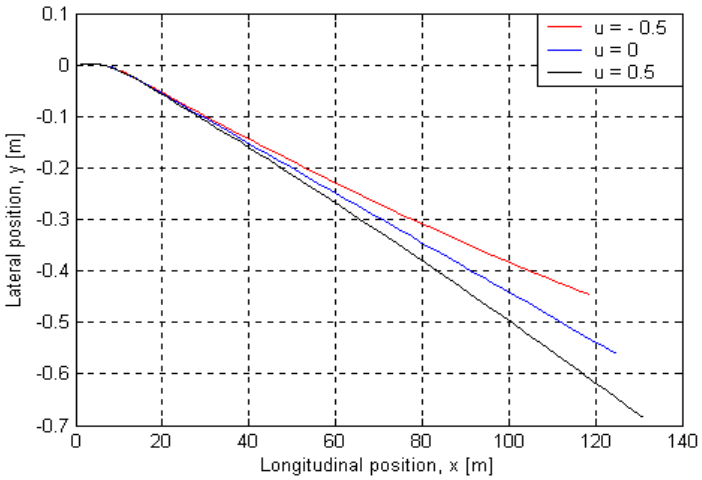


**Figure 5.5:** Trajectory for constant steering angle with initial velocity

### 5.1.3: Zero acceleration with initial velocity:

In the third simulation set, zero longitudinal acceleration is applied to a vehicle traveling with an initial velocity $V_0 = 25m/s$ . For each simulation, the vehicle state responses are obtained and compared for various steering angle inputs. Results for all six states and the vehicle trajectory are given in Figures 5.5 through 5.9. From the plots given in Figure 5.5, the longitudinal velocity decreases for increasing steering angle due to the tire cornering forces that tend to oppose forward motion as the vehicle maneuvers a turn. For a steering angle of 0.1 radians, roughly 6 degrees, the longitudinal velocity drops to 19.5 m/s after 5 seconds. At higher velocity, smaller steering angles should be applied in order to minimize the longitudinal velocity gradient. As shown in Figure 5.6, the vehicle responds quickly to the steering input since the initial velocity is large. The vehicle again begins by moving in the opposite direction of that desired as it first swerves in the positive y-direction for the initial 0.3 seconds. The vehicle then moves in the negative y-direction, as desired. For a steering

angle of 0.01 radians, roughly 0.6 degrees, the lateral velocity reaches a steady-state value of –0.15 m/s after 1 second.

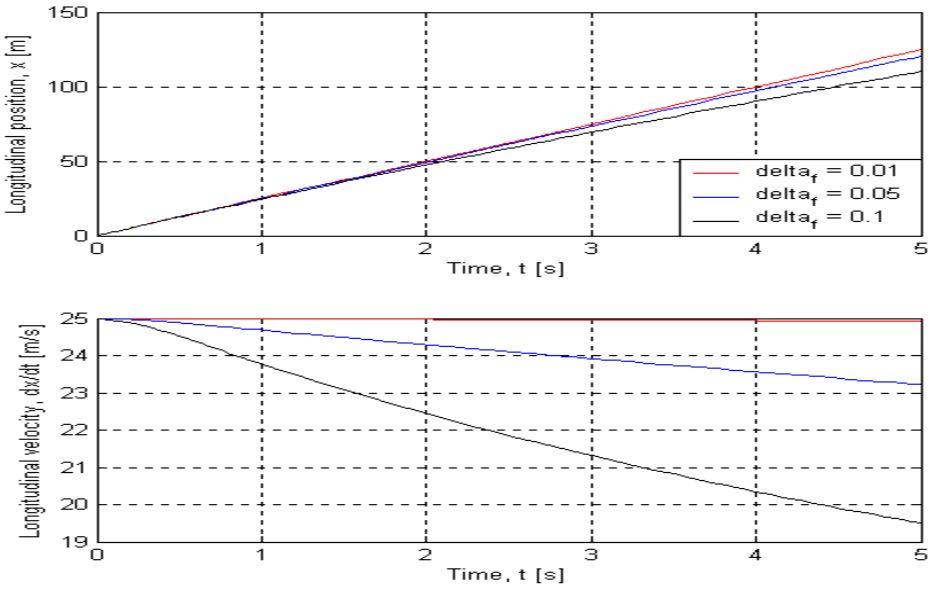


**Figure 5.6:** Longitudinal response for zero acceleration and initial velocity

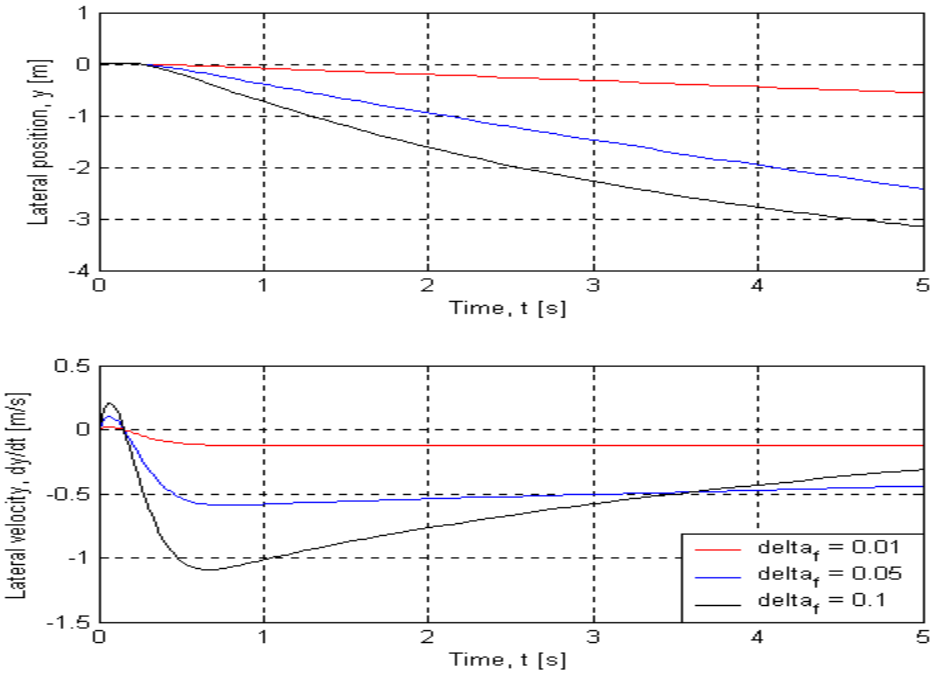


**Figure 5.7:** Lateral response for zero acceleration and initial velocity

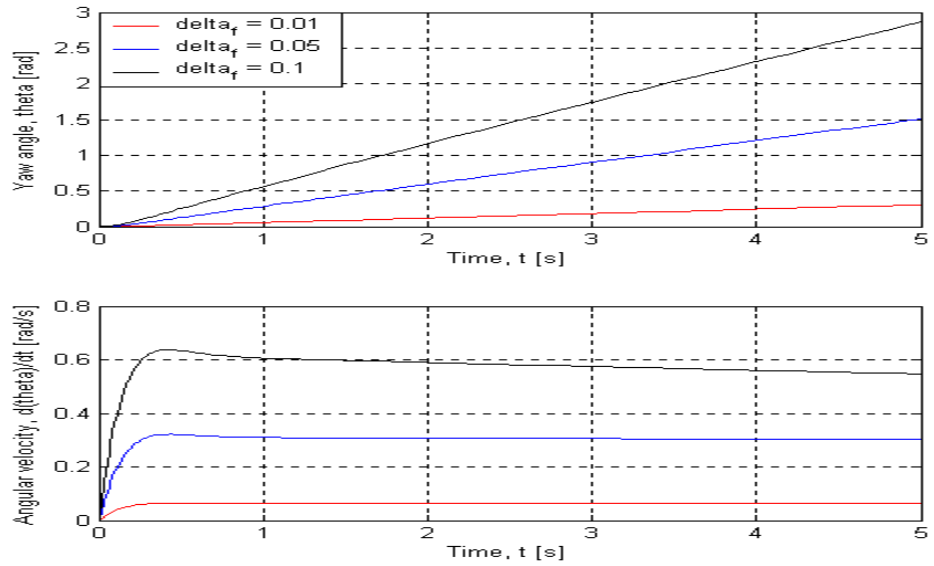


**Figure 5.8:** Angular response for zero acceleration and initial velocity

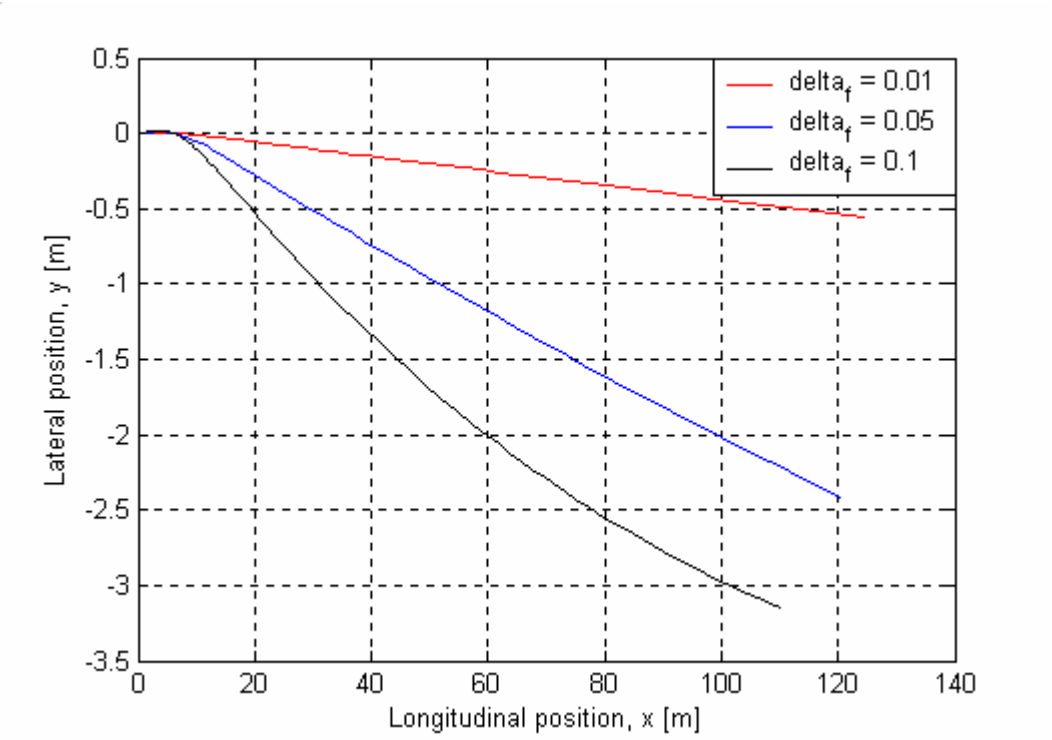


**Figure 5.9:** Trajectory for zero acceleration and initial velocity

From the plots given in Figure 5.8, the yaw angle is roughly linear over time for all three steering angles. For the smaller steering angle of 0.01 radians, the angular velocity response reaches a steady state value of 0.06 rad/s after 0.25 seconds while the angular velocity response exhibits an initial peak at about 0.3 seconds for larger steering angles before approaching its final value. As shown in Figure 4.14, after 5 seconds, the vehicle has traveled a longitudinal distance of roughly 120 m. The difference in lateral position between the small and larger steering angles is more significant, almost 3 m after 5 seconds. Steering angles of less than 0.1 radians are more suitable for turning and lane-changing maneuvers.

Another simulation was performed in order to get how the slip angle varies, for that XUV was simulated with the same parameters as used in the table and the Equations of motion taken into consideration were (3.1), (3.2), (3.3),(3.4), (3.5),(3.6),(3.7), (3.8) .

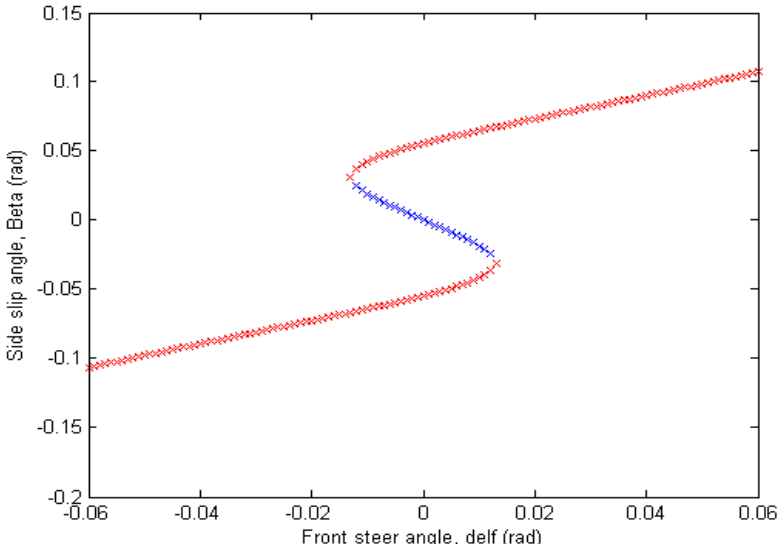


**Figure 5.10:** Front Steering angle Vs Side Slip angle
Velocity = 40m/s ; Steering angle = 0.015 radians

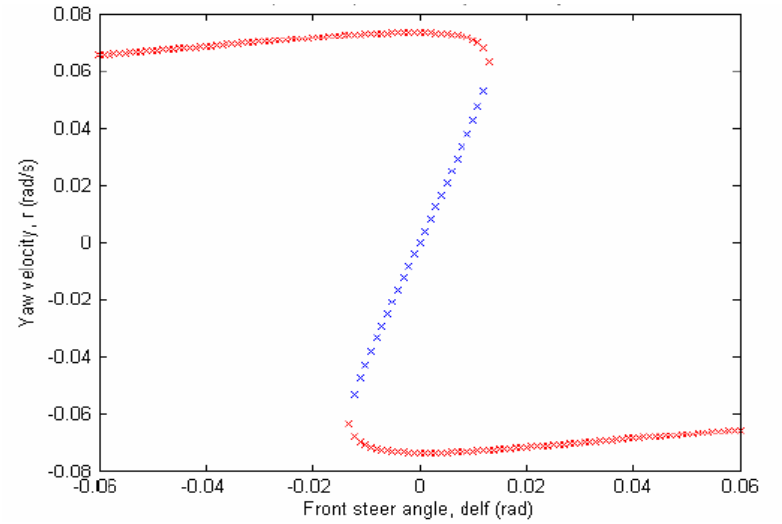


**Figure 5.11:** Front Steering angle Vs Yaw Velocity
Velocity = 40m/s; Steering angle = 0.015 radians

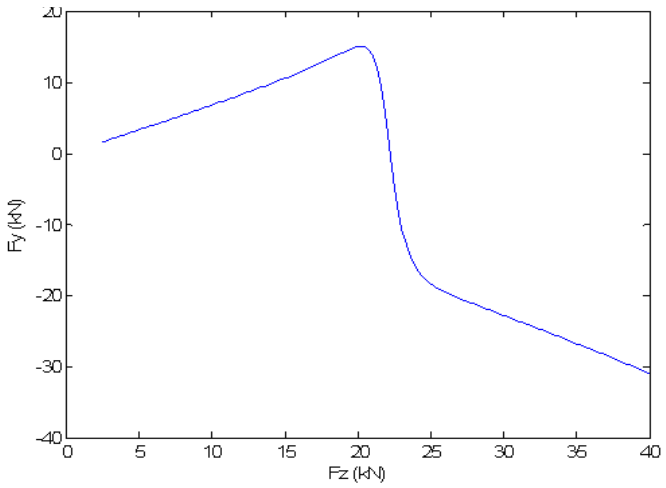


**Figure 5.12:** Lateral force Vs vertical Load at -60 deg slip angle.

### 5.2 Dynamic analysis for XUV steering using ADAMS:

Mobile robots are being used for military reconnaissance, rough terrain application, and space exploration. In all the robotic application robots need to have high maneuverability and a very sturdy steering system .Steering system used for the robotic vehicles is the same as it is used in automobiles except the robotic vehicles are autonomous .It is seen that little research has been done which takes care of the dynamic aspect of the vehicle .

In chapter 4, the bicycle model for the four wheel steering vehicle was developed and vehicle handling characteristics were discussed using matlab simulations. In this section ADAMS was used to simulate the vehicle model .The 3d vehicle model of the XUV is developed in ADAMS. The ratio of rear wheel steering to front wheel steering used here is 0 as it is a front wheel steering.

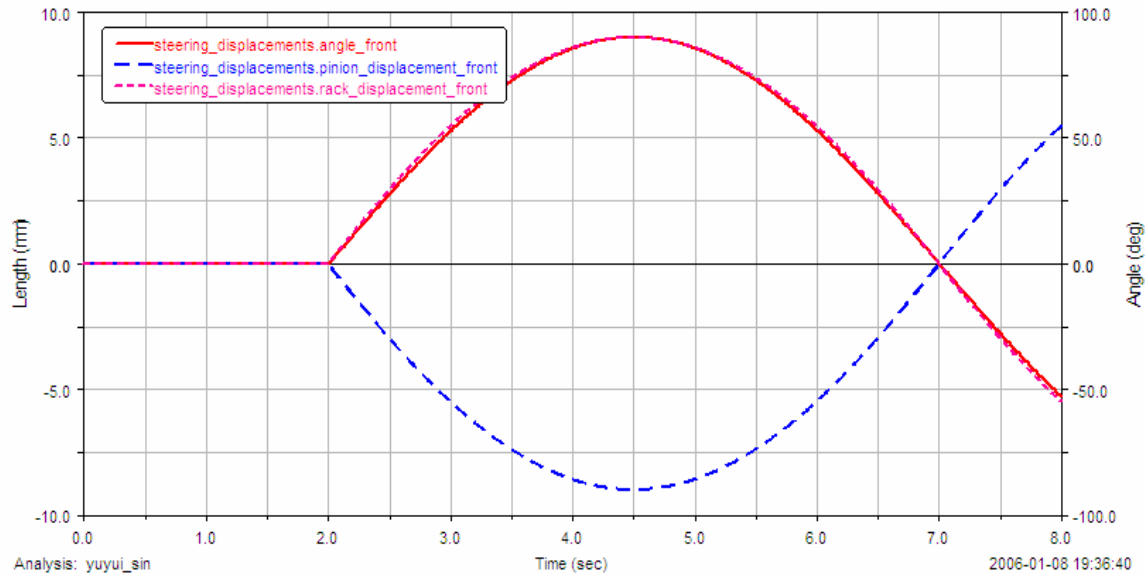


**Figure 5.13:** Steering Displacement Vs time

Rack pinion Vs time

Pinion displacement Vs time

This figure describes the variation of steering vs time, rack pinion vs time and the pinion displacement vs time.

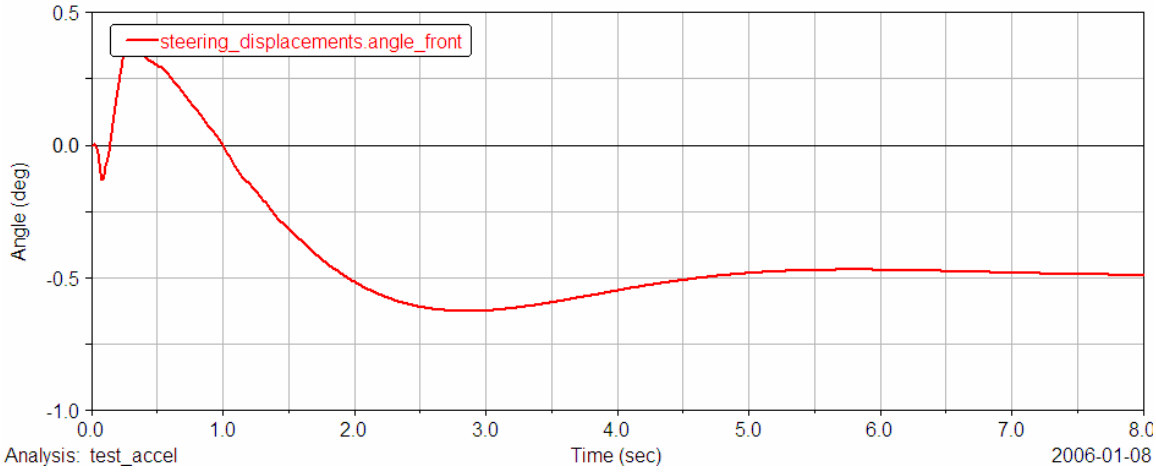


**Figure 5.14**: Front steering angle Vs time

In the figure 5.11 shows the front steering angle response which is initially positive and then goes negative as the vehicle makes a turn, this can be compared to the graph obtained from mat lab, although the graphs are not identical but the trajectories of the graph are the same.

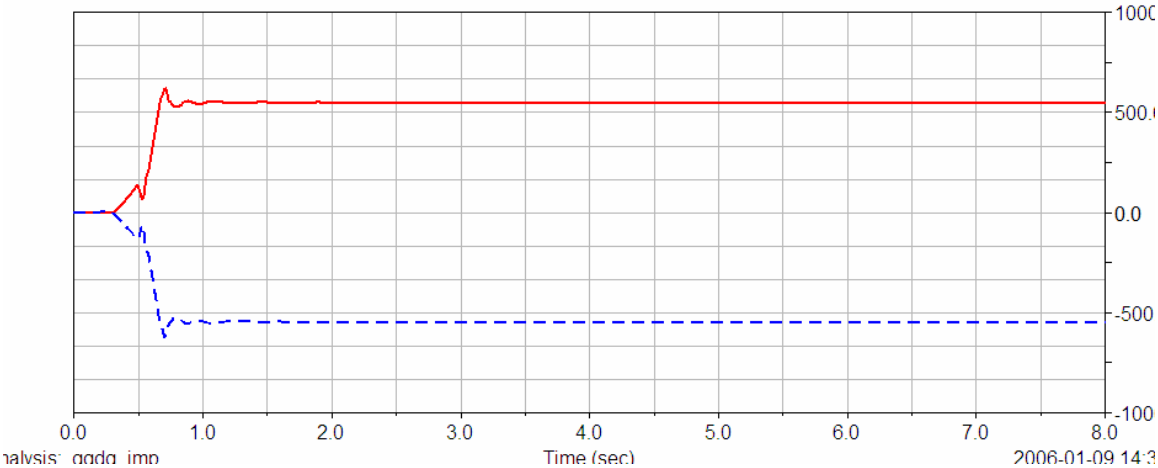


**Figure 5.15:** Comparison of the front and rear steering angle response for a 30 degree turn

Figure 5.15 It gives the Comparison of the front and the rear steering angle response if the XUV is maneuvered on a 30 degree turn.

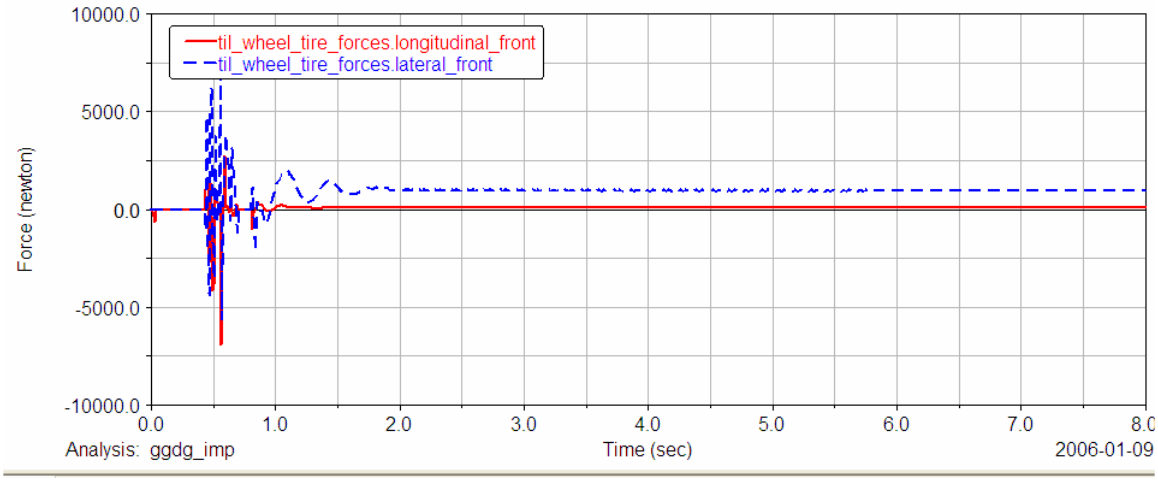


**Figure 5.16:** Front Longitudinal and Lateral Force response for XUV for a 30 degree impulse steer

Figure 5.13 shows the lateral and longitudinal force response for XUV which is maneuvered for a 30 degree turn.

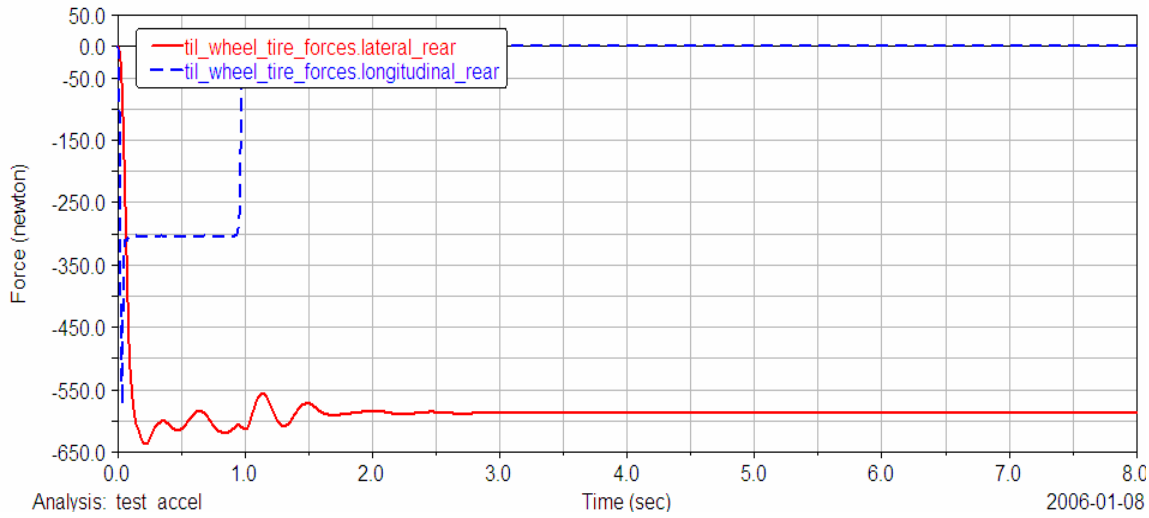


**Figure 5.17:** Lateral and Longitudinal Rear tire forces

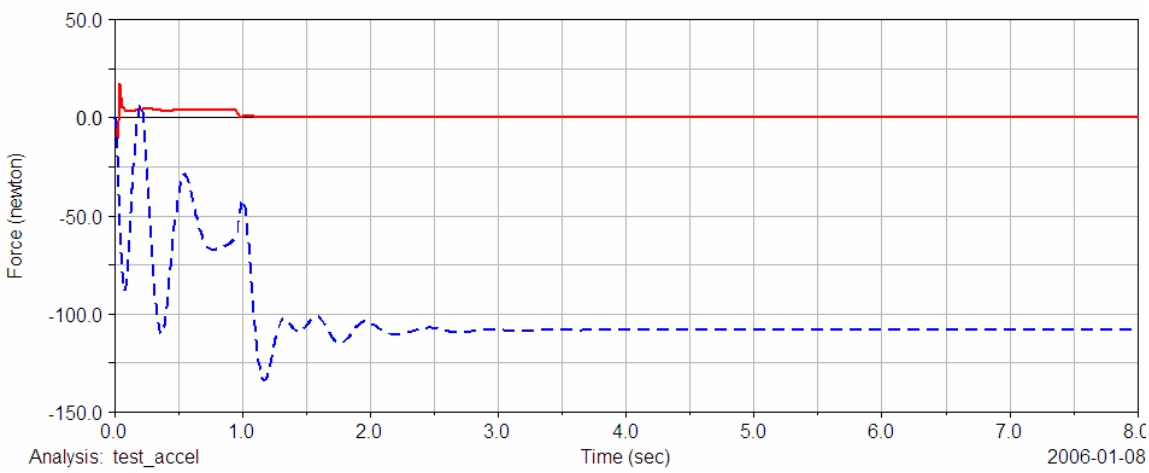


**Figure 5.18:** Front lateral and longitudinal tire force response

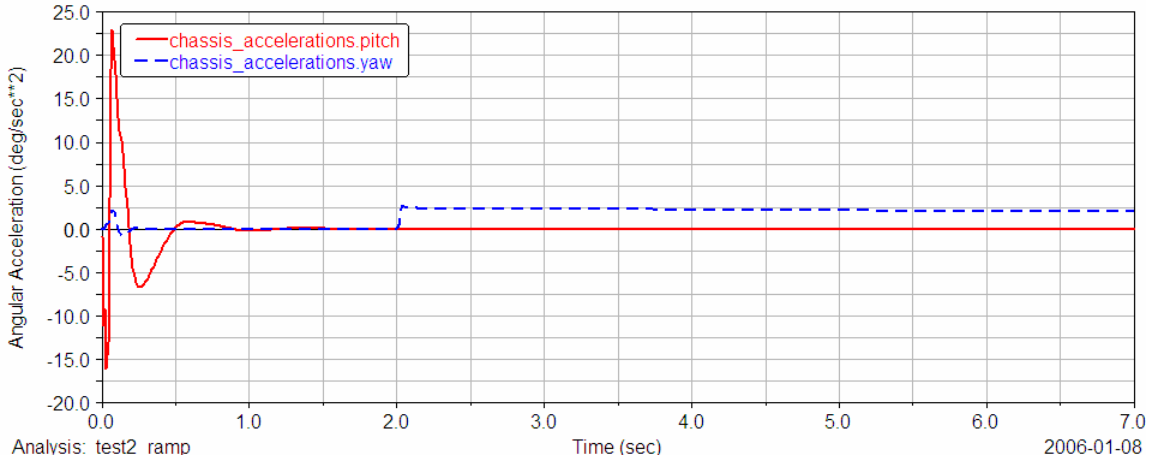


**Figure 5.19:** Pitch and yaw response for XUV turning at 30 degree turn

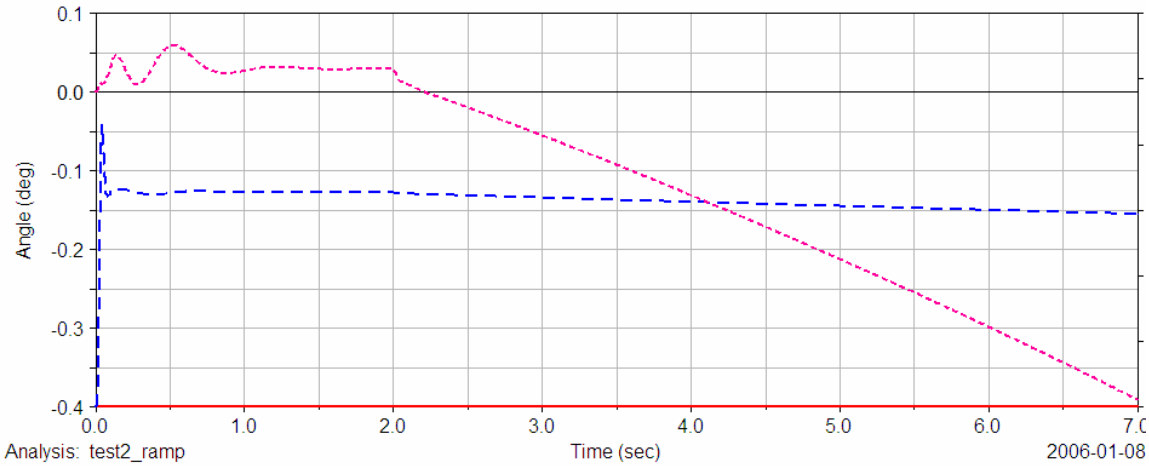


**Figure 5.20:** Lateral and longitudinal Slip angle response of XUV for a 30 degree turn maneuver

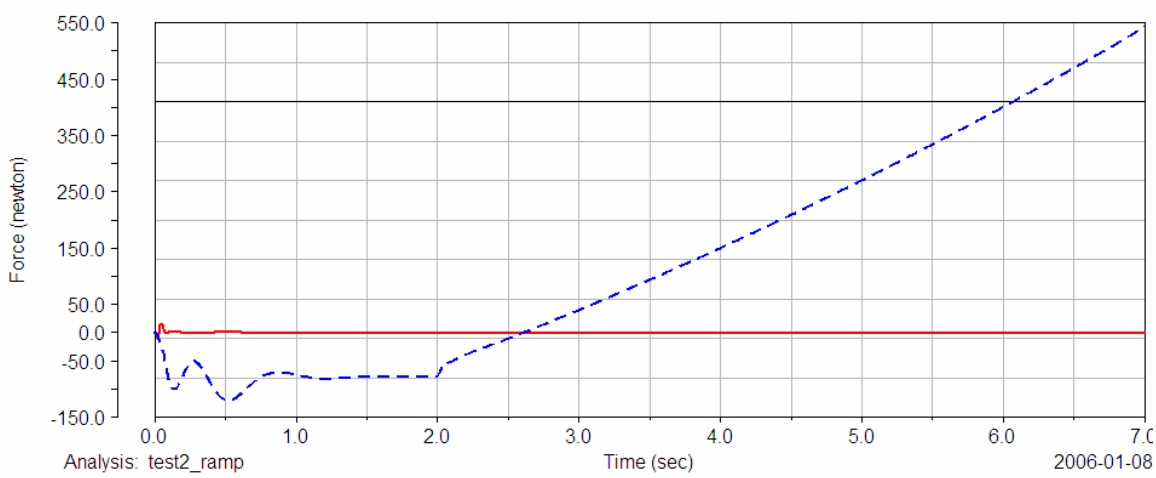


**Figure 5.21:** Front lateral and longitudinal force response for XUV

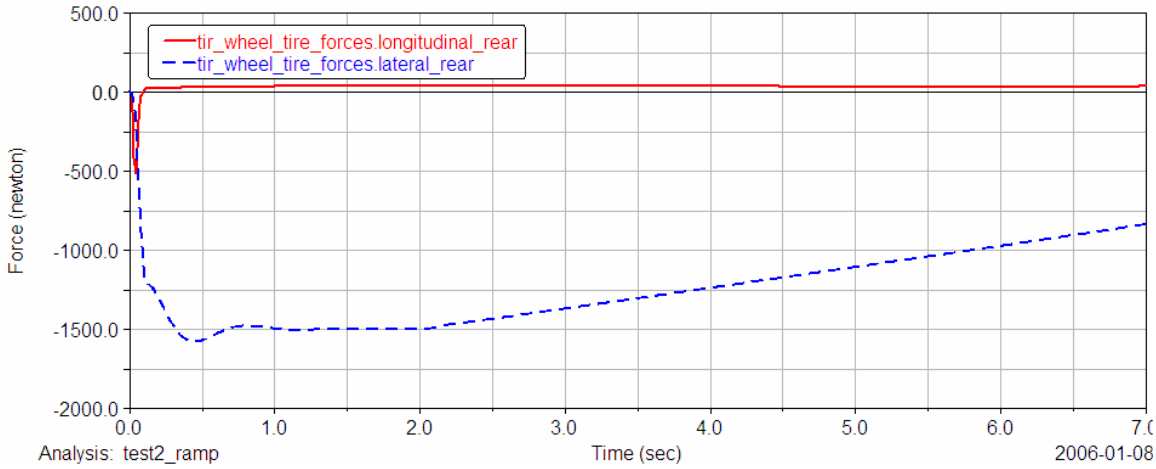


**Figure 5.22:** Rear lateral and longitudinal force responses for XUV during a 30 degree turn

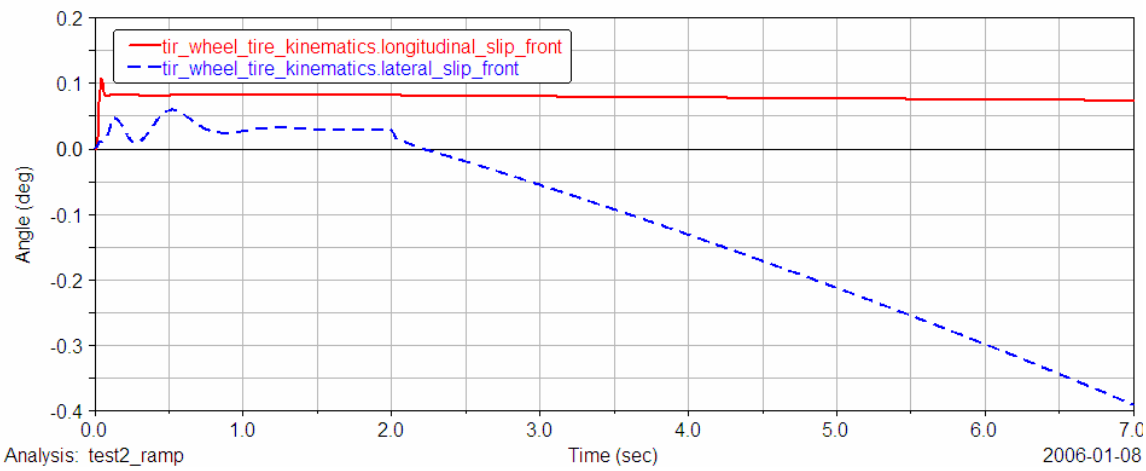


**Figure 5.23:** Longitudinal and lateral front slip angle response of XUV for a 30 degree ramp steer

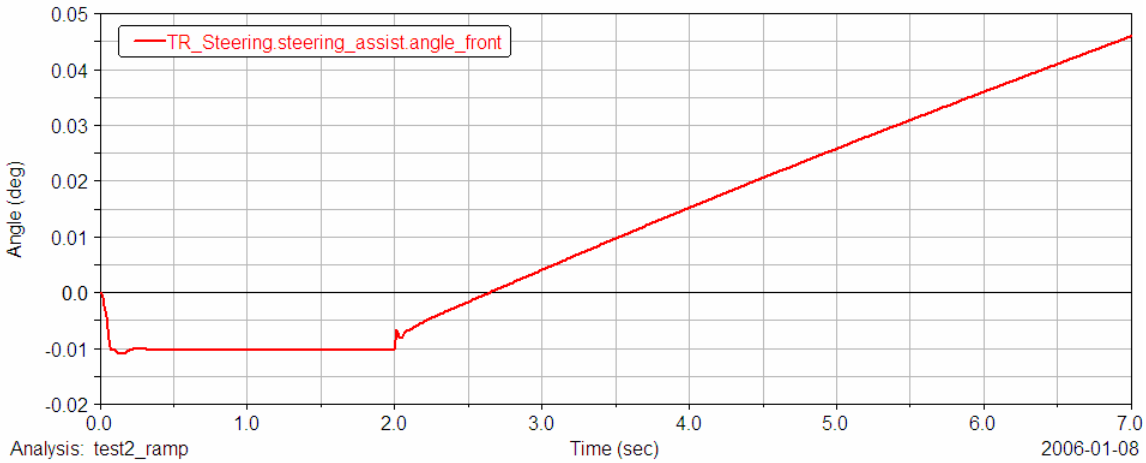


**Figure 5.24:** Steering angle Vs time during a 30 degree turn in XUV

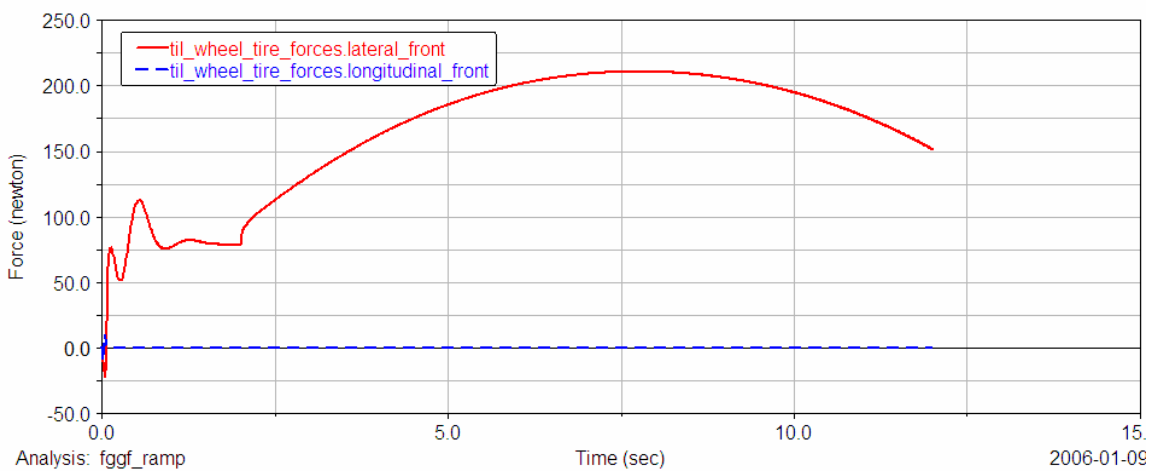


**Figure 5.25:** Longitudinal and lateral front forces for a 90 degree impulse steer in an XUV

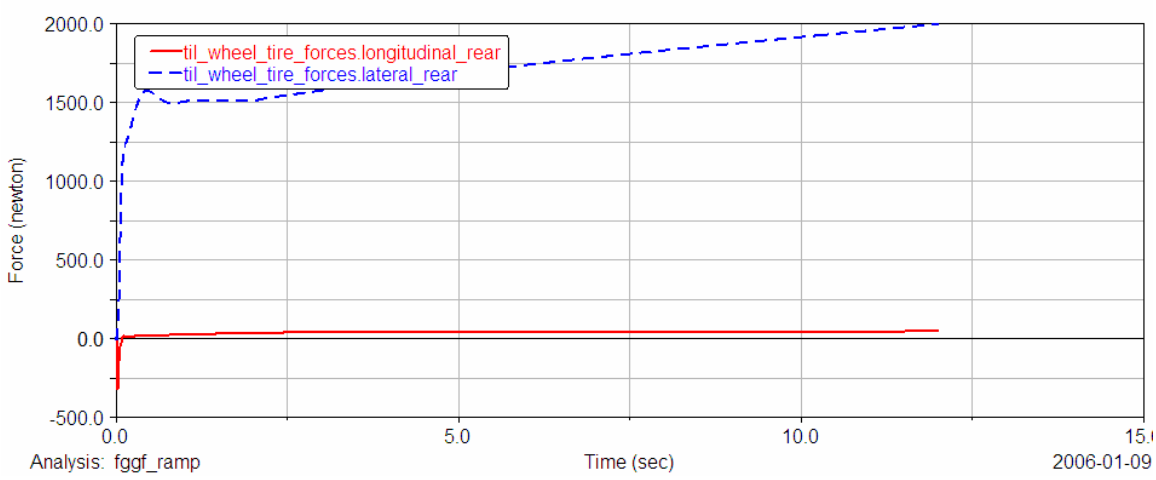


**Figure 5.26:** Longitudinal and lateral rear forces for XUV during a 90 degree impulse steer

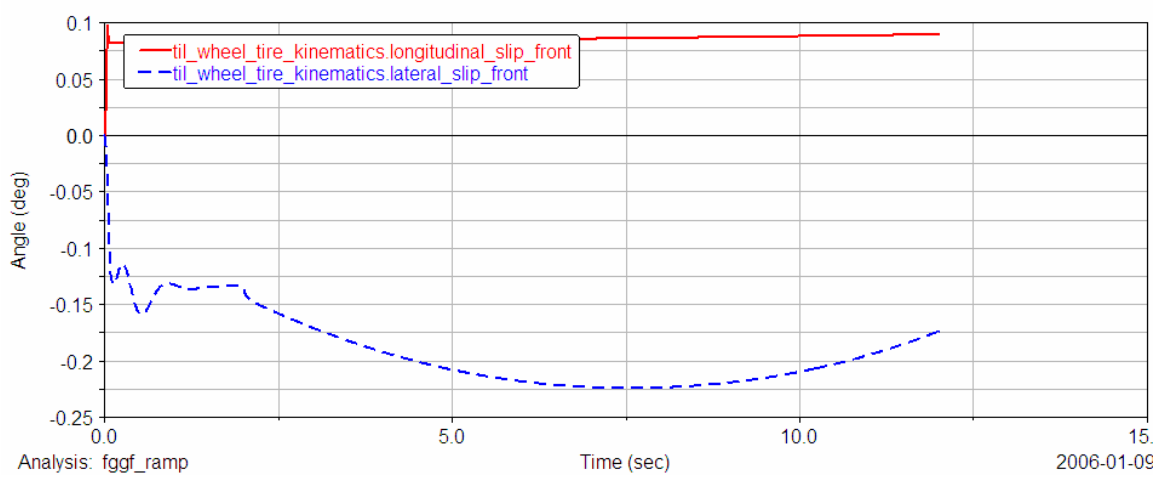


**Figure 5.27:** Longitudinal and lateral front slip angles for a 90 degree ramp steer for an XUV

## Conclusion:

A mathematical model of the Steering System used in Xuv was derived, and the simulation in matlab were performed in order to know how the vehicle is going to behave On various terrains by simulating it for different conditions .At the same time dynamic simulations were performed in ADAMS on XUV model using the same parameters and the results were captured. Considering the kind of terrain on which the XUV is going to operate, it requires a more stable kind of Steering system as for a rough terrain it requires a vehicle to have more power and on that tire wear will be more. Further the model was linearized and simplified to form the bicycle model for the lateral dynamics and non linear model of tire was discussed , effects of the road banked on the vehicle lateral dynamics was noted.

Then a controller was modeled using the dynamic equations of motion and the equations of electric motor which in this case is considered the prime means of motion of XUV in Order to modulate the speeds, then the effect of the sampling time on the response of the Vehicle is studied. The ADAMS Program was used for modeling, simulation, testing and animation of different simulation conditions and the vehicle stability was discussed.
Then the vehicle's yaw rate, steering angle, roll motion, lateral acceleration, are discussed. These results form the basis for more complex model development and mechanism design for future research.

This thesis is useful in the following areas:

1) Different type of steering system used in robotic vehicles
2) Analytical modeling of bicycle model in Matlab.
3) Dynamic modeling of XUV in ADAMS.

.

# FUTURE RESEARCH

This research presented a new method to study vehicle handing performance. Vehicle models evolved from a simple bicycle model to models allowing for wide operating ranges and lateral load transfer. In addition to characterizing vehicle handing performance, this method can also be used (to an extent) to predict vehicle motions for particular steering maneuvers.

## Recommendations for future work:

Reformulating a vehicle model to allow for drive torque and combined slip Effects (lateral and longitudinal).The Vehicle Model developed here is without suspension system. Suspension characteristics need to be taken into account .Right now the Matlab simulation and the ADAMS simulation do not match each other closely, so the mathematical model needs to be refined by taking into account the pitch motion.

# APPENDIX

## B.1 Initial.m

```
% This subprogram initializes the Xuv and inputs
global theta0;


%%%%%%%%%%%%%%%%%% Simulation Control Constants %%%%%%%%%%%%
control = 1; %Chooses which controllers are used
% 0 = Velocity controller without lateral controller
% 1 = Dynamic velocity and lateral controller, THIS IS THE FULL CONTROLLER
% 2 = Truncated velocity controller and Lateral controller
% 3 = No dynamic controllers, just kinematic controllers
plot_me = 1; %Chooses what plots to show
% 0 = No plots
% 1 = plots all data for control=1 - must be Full Controller
% 2 = plots all data for control~=1 - does not work for Full Controller
% 3 = plots comparisons of kinematic controllers to dynamic controllers
% run the full controller second
show_me = 1; %Shows the movie 0=off 1=on
%Control gains
k1 = 2000; % The first three are for the lateral controller
k2 = 100;
k3 = 100;
kv1 = 5; % The last two are for the speed controller
kv2 = 1250;
```



```
% Define's the path
x_path=[-2.5:.01:2.5];
[y_path,path_fun]=F_path(x_path);
% Initial conditions (must be on the road!!!)
init_x = -1.14;
x0 = init_x; % position of center of rear wheels along the x axis (m)
```

```
dx0 = x0+T; % for setting theta0
x = x0;
y0 = eval(path_fun); % position of center of rear wheels along the y axis (m)
x = dx0;
dy0 = eval(path_fun); % for setting theta0
theta0 = atan2(dy0-y0,dx0-x0); % body angle (rad)
phi0 = 0*pi/180; % steering angle (limited -45 to 45 degrees) (rad)



vu0 = .5;
Fd0 = 0;
vd = 1.0; %desired velocity, in m/s actual speed (not scale)
d_vd = 0; %dvd = diff(vd);
mph = vd*0.62137*36 %desired full scale speed
u2 = 0; % v2 transformed (rad/s)
%Sets the scene and viewpoint of the movie
if show_me == 1
axis equal;
grid on;axis([x0-2*W -x0+2*W y0-l -y0+l]);
%axis off;
view(2);
%view(3);
end
%initializing other variables
theta0_prev = theta0;
phi0_prev = phi0;
PHI = phi0;
FD = Fd0;
c = phi0;
prev_front = 0;
prev_back = 0;
% create Xuv and locate it on the road
if show_me == 1
```



```
hold on
Xuv = Create Xuv (W,l,H,D,F,R,b,'green');
locate(Xuv,[x0 y0 0]);
aim(Xuv,[x0+cos(theta0) y0+sin(theta0) 0]);
turn(Xuv.tire_fl,'z',phi0*180/pi);
turn(Xuv.tire_fr,'z',phi0*180/pi);
end
```

# B.2 constants.m

```
% Constants for the Xuv
l = 10 *2.54/100; % distance between rear wheel and front wheel (m)
W = 6.5 *2.54/100; % space between wheels (m)
H = 6 *2.54/100/2; % height (m)
D = 2.5 *2.54/100; % diameter of wheels (m)
F = 1.25 *2.54/100; % width of front wheels (m)
R = 2 *2.54/100; % width of rear wheels (m)
B_w = 5 *2.54/100;
T = 0.01; % sampling time (s)
b = 3.5 *2.54/100; % distance from CG to rear axle
a = l-b; % distance from CG to front axle
sensors = 16;
Ra = 1.9;
La = 1.064e-4;
Nw = 81;
Nm = 21;
Rw = 31.75e-3;
bm = 3.397e-5;
Km = 6.7831e-3;
Kb = Km;
m = 1.4175;
J = W*l*m;
Jeq = b^2*m+J;
% use numerical integration and plot

% steering for bicycle model of car

% init condx [theta ya xb yb]

L = 0.3;     % XUV length m

theta = 0.0; ya = 0.25; % parallel to line, 0.25 m offset

xb = -L * cos(theta); yb =ya +L * sin(theta);

y0 = [theta ya xb yb];

t0 = 0.0;   tf = 5;

tspan = [t0 tf]; % simulate for 20 seconds

[t,y] = ode45('bicycle',tspan,y0);

% You can try ode15s if you have any problems on ode45.

y1=y(:,1);  % orientation wrt line

y2=y(:,2);  % offset wrt line of front of XUV

y3=y(:,3);  % longitudinal position of back of XUV

y4=y(:,4);  % lateral posiiton of back of XUV


plot(y3,y4);
```

# REFERENCES


[1] N.J. Nilson, A Mobile Automation :An application of Artificial Intelligence Techniques, Proc. IJCAI, Washington DC, 1969.

[2] A.M. Thompson, The Navigation System of the JPL Robot, Proceedings Fifth IJCAI, Cambridge MA, 1977.

[3] Hans Moravec, Visual Mapping by a Robot Rover, Proc. 6th IJCAI, Tokyo, 1979.

[4] http://iirobotics.com/webpages/robohistory.php

[5] Muirhead B.K., Mars Pathfinder flight system integration and test**,** Aerospace Conference, 1997. Proceedings., IEEE , Volume: 4 , 1-8 Feb. 1997.

[6] Tanie, K, Humanoid robot and its application possibility**,** Multisensor Fusion and Integration for Intelligent Systems, MFI2003. Proceedings of IEEE International Conference on , 30 July-1 Aug. 2003.

[7] Aronson, Z.H., Lechler, T., Reilly, R.R., Shenhar, A.J., Project spirit-a strategic concept**,** Management of Engineering and Technology, 2001. PICMET '01. Portland International Conference on , Volume: 1 , 29 July-2 Aug. 2001.

[8] http://www.mobilerobots.com/patrolbot.html

[9] http://www.irobot.com/consumer/default.asp

[10] Hornby, G.S., Takamura, S, Yokono, J., Hanagata, O., Yamamoto, T., Fujita, M., Evolving robust gaits with AIBO**,** Robotics and Automation, 2000. Proceedings. ICRA '00. IEEE International Conference on , Volume: 3 , 24-28 April 2000.

[11] http://www.army-technology.com/contractors/mines/i_robot/

[12] Huai-yu Wu, Dong Sun, Zhao-ying Zhou, Shen-shu Xiong, Xiao-hao Wang, Micro air vehicle: architecture and implementation, Robotics and Automation,

2003. Proceedings. ICRA '03. IEEE International Conference on, Volume: 1, 14-19 Sept. 2003.

[13] http://www.machinebrain.com/Fighting_Robots/Military_Robots/more2.html

[14] R. M. Desantis. *Path-Tracking for Car-Like Robots with Single and Double Steering*.
IEEE Tran. Veh. Technol. Vol. 4, No. 2, May 1995.

[15] Thomas D. Gillespie, "Fundamentals of Vehicle Dynamics" Third Edition, S. A. E.

[16] M. Egerstedt, et al. *Control of a Car-Like Robot Using a Dynamic Model*. IEEE Conference
on Robotics and Automation. May 1998.

[17] K. Park, et al. *Point Stabilization of Mobile Robots Via State Space Exact Feedback Linearization*. IEEE Conference on Robotics and Automation. May 1999.

[18] S. Lee, et al. *Control of Car-like Mobile Robots for Posture Stabilization*. IEEE Conference
on Intelligent Robots and Systems. 1999.

[19] P. Kachroo. *Nonlinear Control Strategies and Vehicle Traction Control*. Dissertation.
University of California, Berkeley, 1993.

[20] P. Mellodge. *Feedback Control for a Path Following Robotic Car*. Thesis. Virginia Polytechnic
Institute and State University, 2002.

[21] R. D. Henry. *Automatic Ultrasonic Headway Control for a Scaled Robotic Car*. Thesis.
Virginia Polytechnic Institute and State University, 2001.

[22] "Vehicle steering study" Degree Project by Sebastien Feve and Alexandre Huret D Georgia Institute of Technology , June 1999.

[23] Shin-ichiro Sakai, Hideo Sado, and Yoichi Hori, "Motion Control in an Electric Vehicle with 4 Independently Driven In-Wheel Motors" IEEE Trans. on Mechatronics, Vol. 4, No.1, pp.9-16, 1999.3.

[24] Hongchu Qiu, Qin Zhang, John F. Reid, and Duqiang Wu, "Modeling and simulation
of electro-hydraulic steering system" Paper No.: 993076, ASAE Meeting Presentation UILU-ENG-99-7019.

[25] Benjamin Shamah, Michael D. Wagner, Stewart Moorehead, James Teza, and David Wettergreen, "Steering and Control of a Passively Articulated Robot" Sensor Fusion and Decentralized Control in Robotic Systems IV, Vol. 4571, October, 2001.

[26] "Vehicle Dynamics Terminology," SAEJ670E, Society of Automotive Engineers, Warrendale, PA, 1992, Appendix A.

[27] Cole, D.E., *Elementary Vehicle Dynamics*, Department of Mechanical Engineering, University of Michigan, Ann Arbor, MI, 1971.

[28] Wong, J.Y., *Theory of Ground Vehicles*, Wiley-Interscience, Ottawa, Ontario, 1978, p. 216.

# BIOGRAPHICAL SKETCH

Saurabh Malhotra was born on December 29th , 1980 in Gurgaon , (Haryana ) India. He obtained his Bachelor's in Mechanical Engineering from University of Haryana , India. He obtained the degree with first class with Distinction. While at University of Haryana, Saurabh gained valuable experience through the Cooperative Education Program by working at Krishna Maruti Ltd, Gurgaon, India. He gained experience in reliability support engineering, product development. After working for 1 year he moved to Florida state university to pursue his masters in Mechanical Engineering .He worked with Dr hollis and his team for the project called CISCOR.